JEM Journal of Experimental Medicine

ARTICLE

JAML promotes CD8 and γδ T cell antitumor immunity and is a novel target for cancer immunotherapy

Joseph M. McGraw[1,2], Flavian Thelen[1], Eric N. Hampton[2], Nelson E. Bruno[2], Travis S. Young[2], Wendy L. Havran[1], and Deborah A. Witherden[1]

T cells are critical mediators of antitumor immunity and a major target for cancer immunotherapy. Antibody blockade of inhibitory receptors such as PD-1 can partially restore the activity of tumor-infiltrating lymphocytes (TILs). However, the activation signals required to promote TIL responses are less well characterized. Here we show that the antitumor activity of CD8 and γδ TIL is supported by interactions between junctional adhesion molecule–like protein (JAML) on T cells and its ligand coxsackie and adenovirus receptor (CXADR) within tumor tissue. Loss of JAML through knockout in mice resulted in accelerated tumor growth that was associated with an impaired γδ TIL response and increased CD8 TIL dysfunction. In mouse tumor models, therapeutic treatment with an agonistic anti-JAML antibody inhibited tumor growth, improved γδ TIL activation, decreased markers of CD8 TIL dysfunction, and significantly improved response to anti–PD-1 checkpoint blockade. Thus, JAML represents a novel therapeutic target to enhance both CD8 and γδ TIL immunity.

Introduction

Functional impairment of T cells within the tumor microenvironment (TME) is a hallmark of cancer progression (Thommen and Schumacher, 2018). Immune checkpoint blockade targeting inhibitory receptors such as programmed cell death protein 1 (PD-1) and CTLA-4 can partially restore tumor-infiltrating lymphocyte (TIL) activity within the tumor and improve patient outcomes. In patients with metastatic melanoma, treatment with a combination of ipilimumab (anti–CTLA-4) and nivolumab (anti–PD-1) improves the median overall survival to >5 yr versus an average of <1 yr in patients treated with chemotherapy or high-dose IL-2 (Larkin et al., 2015; Larkin et al., 2019; Postow et al., 2015, Garbe et al., 2011). Despite improvement in this population, nearly half of metastatic melanoma patients do not respond to checkpoint blockade therapy, and response rates in other cancers, such as prostate and brain cancer, are far lower (Chen and Mellman, 2017; Chen et al., 2020). Therefore, there is a critical unmet need to identify additional mechanisms of T cell–mediated tumor immunity that can be leveraged to improve response rates.

Although much research has focused on CD4 and CD8 T cells as central targets of cancer immunotherapy, more recently, the critical role of other immune cell subsets, such as γδ T cells, has been elucidated (Silva-Santos et al., 2019). γδ T cells are a minor population within lymphoid tissues (~1–5% of T cells in peripheral blood) but are present in larger numbers in both mouse and human epithelial tissues (10–100% of T cells) such as the skin and gut (Nielsen et al., 2017). These tissue-resident γδ T cells are important for maintaining epithelial homeostasis and for the response to tissue damage via recognition of self-stress molecules, independent of MHC antigen presentation (Nielsen et al., 2017). Compared with all other leukocyte populations, increased γδ T cell tumor infiltration is the best prognostic factor of improved patient survival across a variety of cancer types, highlighting their critical role in antitumor immunity (Gentles et al., 2015). Furthermore, mice lacking γδ T cells (*Tcrd*$^{-/-}$) are more susceptible to both spontaneous and transplantable tumor models (Silva-Santos et al., 2019). Mechanistically, γδ T cells have been shown to provide an early source of IFNγ within tumors that supports αβ TIL responses and helps limit tumor formation (Girardi et al., 2001; Gao et al., 2003). In this way, γδ T cells may serve as a bridge between the innate and

[1]Department of Immunology and Microbiology, The Scripps Research Institute, La Jolla, CA; [2]Department of Biology, California Institute for Biomedical Research at The Scripps Research Institute, La Jolla, CA.

Correspondence to Deborah A. Witherden: deborahw@scripps.edu; Travis S. Young: youngtr@scripps.edu

W.L. Havran died in January 2020.

adaptive immune systems. However, the exact mechanisms that mediate γδ T cell responses to tumors are not well characterized.

Junctional adhesion molecule–like protein (JAML; also known as AMICA1 in humans) is a member of the JAM family and is expressed by monocytes, neutrophils, activated CD8 T cells, and tissue-resident γδ T cells (Luissint et al., 2008; Moog-Lutz et al., 2003; Witherden et al., 2010). JAM family members facilitate tight junction assembly; regulate leukocyte–endothelium interactions; and have diverse roles in development, angiogenesis, inflammation, and cancer (Kummer and Ebnet, 2018; Lauko et al., 2020). We previously identified JAML as a novel costimulatory receptor that is required for activation of dendritic epidermal T cells (DETCs) in mouse skin, a prototypic tissue-resident γδ T cell population (Witherden et al., 2010). Upon binding to its cognate ligand, coxsackie and adenovirus receptor (CXADR), a cell adhesion molecule expressed on non-hematopoietic cells, JAML induces a phosphoinositide 3-kinase (PI3K) signaling cascade, which promotes DETC activation and proliferation (Verdino et al., 2010; Witherden et al., 2010; Ortiz-Zapater et al., 2017). During cutaneous wound healing, epithelial cells increase expression of CXADR to induce JAML-mediated expression of keratinocyte growth factor 1 from DETCs, which promotes the wound repair process (Witherden et al., 2010). Although prior studies have defined a role for JAML in facilitating tissue trafficking of immune cell subsets (Guo et al., 2009; Zen et al., 2005) and, separately, loss of CXADR expression has been associated with epithelial–mesenchymal transition and metastasis in certain tumor types (Reeh et al., 2013; Nilchian et al., 2019; Anders et al., 2009; Yamashita et al., 2007), a role for JAML–CXADR interactions in antitumor immunity has yet to be described.

Here we show that JAML expression plays a vital role in maintaining effective function of CD8 and γδ T cells within tumors. JAML-deficient (*Jaml*$^{-/-}$) mice are more susceptible to B16F10 melanoma formation and exhibit more aggressive tumor growth. We show that this defect is due to an impaired critical early response of γδ T cells, which is associated with functional exhaustion of CD8 T cells characterized by increased expression of PD-1 and eomesodermin (Eomes) and a decrease in TNFα and IFNγ production. Furthermore, we demonstrate that therapeutic treatment with an agonist anti-JAML mAb (HL4E10) improves activation of CD8 and γδ TILs, resulting in inhibition of tumor growth and enhancement of PD-1 blockade. Collectively, this work identifies JAML as a promising target for cancer immunotherapy.

Results

High expression of JAML is associated with improved patient survival

To assess if JAML–CXADR interactions are potentially prognostic in human cancers, we analyzed The Cancer Genome Atlas (TCGA) and Prediction of Clinical Outcomes from Genomic Profiles (PRECOG; Gentles et al., 2015) human gene expression datasets for associations of *JAML* expression with clinical patient outcomes. High *JAML* expression was associated with improved patient survival in 8 of 43 TCGA cohorts and in 10 of 39 tumor types in PRECOG, and significant associations were found for head and neck cancer, lung cancer, and melanoma in both datasets (Fig. 1 A). Further analysis of the TCGA melanoma (skin cutaneous melanoma [SKCM]) cohort revealed that *JAML* expression was associated with improved median and overall survival (Fig. 1 B). Importantly, high expression of *JAML* was also associated with improved survival in a study of patients with metastatic melanoma treated with anti–PD-1 antibodies (Liu et al., 2019), supporting a prognostic association with response to immunotherapy (Fig. 1 C). This association of *JAML* expression with patient survival was independent of *CXADR* expression, which was not associated with response to PD-1 in the context of metastatic disease (Fig. S1 A). Together with the known roles of JAML–CXADR interactions in regulating immune responses, these data led us to hypothesize that JAML may be important in the regulation of antitumor immunity.

JAML is highly expressed by intratumoral CD8 and γδ T cells

To determine the expression pattern of JAML during an antitumor immune response, we profiled expression of JAML on immune cell subsets in spleen and B16F10 melanoma tumor tissue isolated from WT C57BL/6J mice (Fig. 1, D and E; flow cytometry gating strategy in Fig. S1 B). By day 15 after tumor challenge, ∼50–70% of both CD8 and γδ TILs expressed JAML, whereas <10% of CD4 TILs displayed JAML expression. In contrast, ∼25% of γδ T cells and very low numbers (<5%) of CD4 and CD8 T cells in the spleens of tumor-bearing mice expressed JAML (Fig. 1 F). Within the myeloid cell compartment, a higher percentage of dendritic cells (DCs; CD11c$^+$MHCII$^+$CD11b$^+$; 50%) expressed JAML within tumor tissue than within spleen tissue (∼10%), whereas ∼30–40% of granulocytes (Ly6G$^+$CD11b$^+$) and 10–20% of monocytes (Ly6C$^+$Ly6G-CD11b$^+$) expressed JAML within both tissues (Fig. 1 F). Only a small proportion of tumor macrophages (F4/80$^+$CD11b$^+$; <3%) expressed JAML (Fig. 1 F). As previously published (He et al., 2010), the majority of γδ TILs were infiltrating, lymphoid Vγ1.1$^+$, and Vγ2$^+$ γδ T cells (Garman nomenclature), and a Vγ1.1$^-$ Vγ2$^-$ γδTCR$^+$ TIL population, absent of Vγ3$^+$ DETCs, was also detected (Fig. S1 C). A large fraction of each of these γδ TIL subsets expressed JAML (Fig. 1 G).

Further analysis revealed that expression of JAML on CD8 and γδ TILs was maintained at similar levels between day 11 and day 15 after tumor challenge and did not correlate with tumor size, suggesting initiation of JAML expression on TILs early in tumor growth (Fig. S1 D). In vitro JAML expression was rapidly up-regulated on splenic CD8 and γδ T cells by 4 h after stimulation with PMA and ionomycin and was maintained through the course of the 48-h experiment (Fig. S1, E and F). In vivo on day 11 after tumor challenge, JAML expression coincided with increased expression of CD69 and Ki67 by γδ TILs but not CD8 TILs (Fig. 1 H). However, JAML expression on CD8 TILs was strongly associated with a decrease in coexpression of PD-1 and Eomes (Fig. 1 I), a phenotype that has been used to identify exhausted T cells (Paley et al., 2012; Li et al., 2018). Additional analysis of published RNA-sequencing data (Mackay et al., 2013) revealed that JAML is also highly expressed by skin and lung tissue–resident memory T cells induced by viral infections (Fig. S1 G). Together, these results show that expression of JAML on T cells is increased during initial T cell activation and is

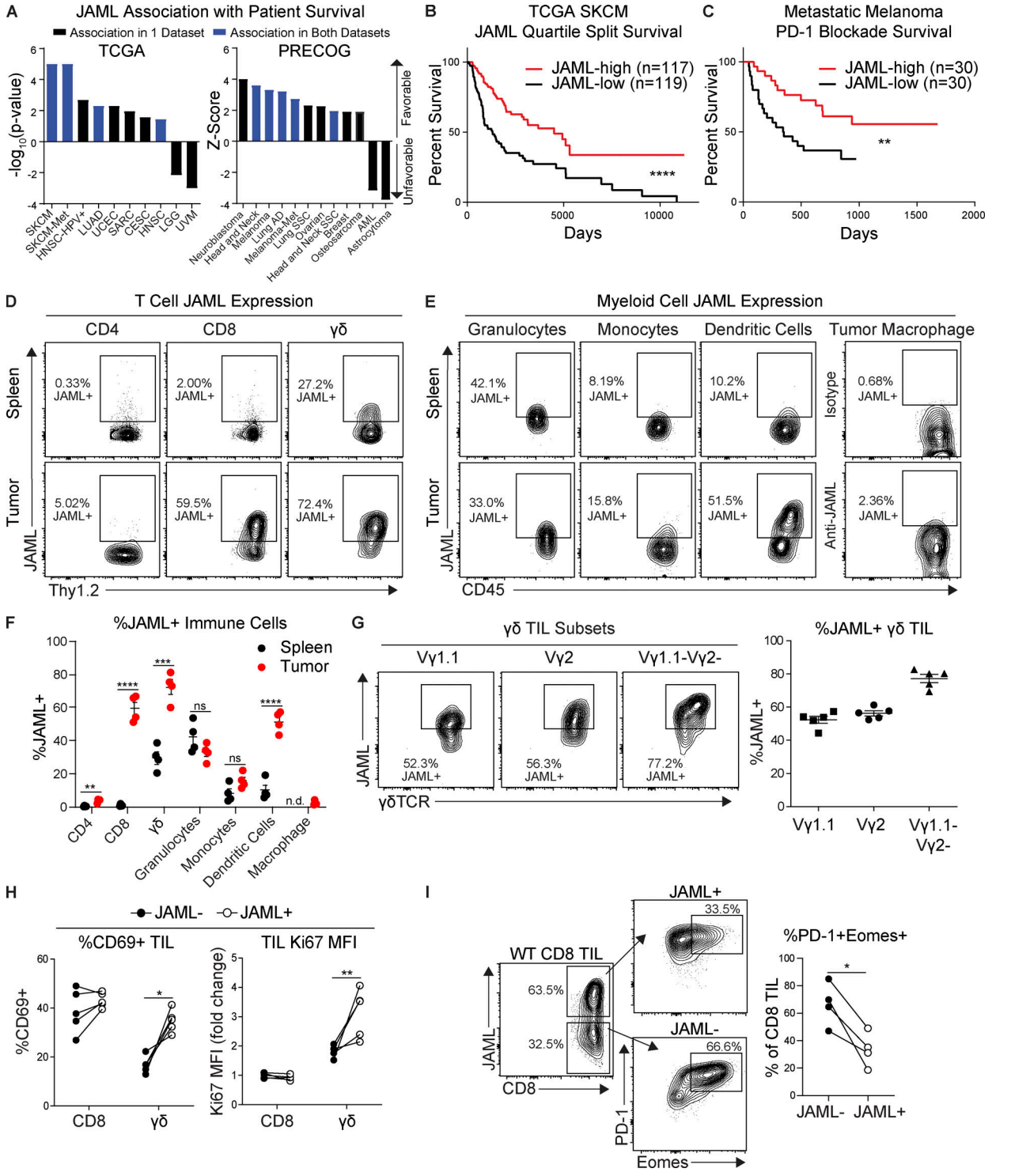

Figure 1. **JAML is associated with improved patient survival and is highly expressed by intratumoral CD8 and γδ T cells in mice. (A–C)** Associations between *JAML* mRNA expression and patient survival were analyzed in publicly available datasets. **(A)** Cancer types in which *JAML* expression is associated with improved patient survival. TCGA, Kaplan-Meier log-rank P values are based on quartile split of *JAML* expression; PRECOG, z-scores of *JAML* association with patient survival. AD, adenocarcinoma; AML, acute myeloid leukemia; CESC, cervical squamous cell carcinoma; HPV, human papillomavirus; HNSC, head and neck squamous cell carcinoma; LGG, low-grade glioma; LUAD, lung adenocarcinoma; Met, metastatic; SARC, sarcoma; SCC, squamous cell carcinoma; UCEC, uterine corpus endometrial carcinoma; UVM, uveal melanoma. **(B and C)** Kaplan-Meier plot of patient survival in (B) TCGA SKCM cohort and (C) anti–PD-1–treated metastatic melanoma based on *JAML* expression. Log-rank P values are shown. **(D–G)** Spleen and B16F10 tumor tissue isolated from WT mice on day 15 after tumor challenge were analyzed by flow cytometry. **(D and E)** Representative flow cytometry plots of T cell (D) and myeloid cell (E) JAML expression. **(F)** Frequency of JAML expression by immune cells (n = 4). **(G)** Representative flow cytometry plots and frequency of JAML expression by Vγ1.1$^+$, Vγ2$^+$, and Vγ1.1$^-$Vγ2$^-$ γδ TIL subsets (n = 5). Data are expressed as mean ± SEM. **(H and I)** B16F10 tumor tissue isolated from WT mice on day 11 after tumor challenge was analyzed by flow cytometry. **(H)** Frequency of CD69 expression and quantification of Ki67 mean fluorescence intensity (MFI; fold change compared with

JAML⁻ CD8 TIL mean) by JAML⁻ and JAML⁺ CD8 and γδ TILs (n = 5). **(I)** Representative flow cytometry plots and frequency of PD-1⁺Eomes⁺ JAML⁻ versus JAML⁺ CD8 TILs (n = 4). Unpaired (F) and paired (H and G) Student's t tests; *, P < 0.05; **, P < 0.01; ***, P < 0.001; ****, P < 0.0001. Data in D–I are representative of a minimum of two independent experiments.

maintained at high levels on T cells within nonlymphoid tissues and the TME.

Jaml$^{-/-}$ mice have a reduced ability to control B16F10 melanoma growth

Next, *Jaml*$^{-/-}$ mice were challenged with B16F10 melanoma, and tumor formation and growth were measured compared with WT animals. After a low tumorigenic dose (10^5 cells), *Jaml*$^{-/-}$ mice developed palpable tumors at a significantly faster rate than WT mice, with 100% of *Jaml*$^{-/-}$ mice developing tumors compared with 50% of WT mice (Fig. 2 A). At a higher tumorigenic dose (5×10^5 cells), tumors exhibited significantly faster growth kinetics in *Jaml*$^{-/-}$ mice than in WT mice (Fig. 2, B and C).

To assess if the increased susceptibility of *Jaml*$^{-/-}$ mice to tumor growth is due to a systemic defect in the T cell compartments, we profiled splenic T cell numbers, phenotypes, and cytokine production in 8-wk-old naive WT and *Jaml*$^{-/-}$ mice. WT and *Jaml*$^{-/-}$ mice had similar numbers of total splenocytes and CD4, CD8, and γδ T cell subsets (Fig. S2, A–D). Similarly, central memory (CD44⁺CD62L⁺) and effector memory (CD44⁺CD62L⁻) T cell compartments were comparable in WT and *Jaml*$^{-/-}$ mice (Fig. S2, E and F). Functionally, T cells isolated from WT and *Jaml*$^{-/-}$ spleens produced similar amounts of TNFα and IFNγ after ex vivo stimulation with PMA and ionomycin (Fig. S2, G and H). Together, these results show that lymphoid T cells in *Jaml*$^{-/-}$ mice do not have any obvious signs of impairment at steady state.

Accumulation of γδ T cells and maintenance of CD8 T cells in tumor tissue are impaired in *Jaml*$^{-/-}$ mice

To understand why *Jaml*$^{-/-}$ mice have impaired antitumor immunity, we characterized the abundance of T cells within the TME on days 11 and 15 after B16F10 tumor challenge by flow cytometry. *Jaml*$^{-/-}$ mice had similar proportions of total CD45⁺ immune cells within tumor tissue compared with WT mice at both time points (Fig. 2 D). On day 11, WT and *Jaml*$^{-/-}$ mice had similar numbers of total T cells, as assessed by Thy1.2 expression (Fig. 2 E). The relative abundance of CD4 and CD8 TILs was similar in WT and *Jaml*$^{-/-}$ at this time point, whereas *Jaml*$^{-/-}$ mice had significantly fewer γδ TILs (Fig. 2, F–H). By day 15, *Jaml*$^{-/-}$ mice had fewer total TILs than WT mice, which was attributable to a decrease in both CD8 and γδ TILs but not CD4 TILs (Fig. 2, E–H). Consistent with a lower abundance of TILs at day 15, CD4, CD8, and γδ TILs in *Jaml*$^{-/-}$ mice expressed a significantly lower amount of Ki67 than TILs in WT mice (Fig. S3, A and B). These results, together with the decreased numbers of CD8 and γδ TILs during tumor growth, suggest that JAML is important for accumulation of γδ T cells and maintenance of CD8 T cell numbers within tumor tissue.

To determine if JAML was involved in myeloid cell infiltration or persistence within the TME, we profiled cell numbers within tumor tissue from WT and *Jaml*$^{-/-}$ mice on day 15 after B16F10 tumor challenge. At this time point, WT and *Jaml*$^{-/-}$ mice had a similar proportion of total CD11b⁺ myeloid cells, granulocytes, monocytes, DCs, and macrophages within tumor tissue (Fig. 2 I), which suggests that JAML–CXADR interactions are not required for myeloid cell tumor infiltration and accumulation. However, potential roles of JAML signaling in other aspects of myeloid cell biology cannot be ruled out.

JAML supports initial γδ T cell activation in response to tumor growth

Given the significant reduction in γδ TIL numbers in *Jaml*$^{-/-}$ mice during early tumor growth on day 11 after tumor challenge compared with WT mice, we additionally sought to characterize γδ TIL subsets and activation levels at this time point. Loss of JAML expression did not preferentially affect the relative frequency of Vγ1.1⁺, Vγ2⁺, or Vγ1.1⁻Vγ2⁻ γδ T cells within the total γδ TIL population, consistent with high expression of JAML on each subset in WT mice (Fig. 3 A). Although a similar percentage of γδ TILs from WT and *Jaml*$^{-/-}$ mice produced IFNγ upon ex vivo stimulation, the relative abundance of IFNγ-producing γδ TILs was decreased in *Jaml*$^{-/-}$ mice compared with WT mice (Fig. 3, B and C), which was associated with significantly lower amounts of T-bet expression (Fig. 3 D). Additionally, γδ TIL expressed similar levels of PD-1 and Eomes in WT and *Jaml*$^{-/-}$ mice and did not coexpress PD-1 and Eomes (Fig. 3, E–G) as observed in CD8 TILs (Fig. 1 G). γδ TILs in WT and *Jaml*$^{-/-}$ mice also expressed similar levels of the proliferation marker Ki67 at this time point (Fig. 3 H). Therefore, although loss of JAML expression by γδ TILs did not alter PD-1, Eomes, or Ki67 expression, the decrease in IFNγ-producing γδ TIL numbers and reduced T-bet expression in *Jaml*$^{-/-}$ mice at this early time point of tumor growth show that the initial activation and tumor infiltration of γδ T cells are impaired in the absence of JAML–CXADR interactions.

Intratumoral CD8 T cells in *Jaml*$^{-/-}$ mice display markers of increased T cell dysfunction

To further characterize CD8 TIL responses in WT versus *Jaml*$^{-/-}$ mice, we analyzed cytokine production following ex vivo stimulation on days 11 and 15 after tumor challenge. *Jaml*$^{-/-}$ mice had a reduced frequency of CD8 TILs that produced TNFα or IFNγ and polyfunctional CD8 TILs producing both TNFα and IFNγ compared with WT mice on day 11, but not day 15, after tumor challenge (Fig. 4 A). A similar fraction of CD4 TILs from WT and *Jaml*$^{-/-}$ mice produced TNFα or IFNγ at both time points (Fig. S4 A). Given the reduced percentage of cytokine-producing CD8 TILs in *Jaml*$^{-/-}$ mice on day 11, we performed additional characterization at this time point and analyzed production of granzyme B and expression of T-bet and Eomes based on recent reports, which have shown that high expression of Eomes and an altered T-bet/Eomes ratio are associated with increased T cell exhaustion (Paley et al., 2012; Li et al., 2018; Lee et al., 2019).

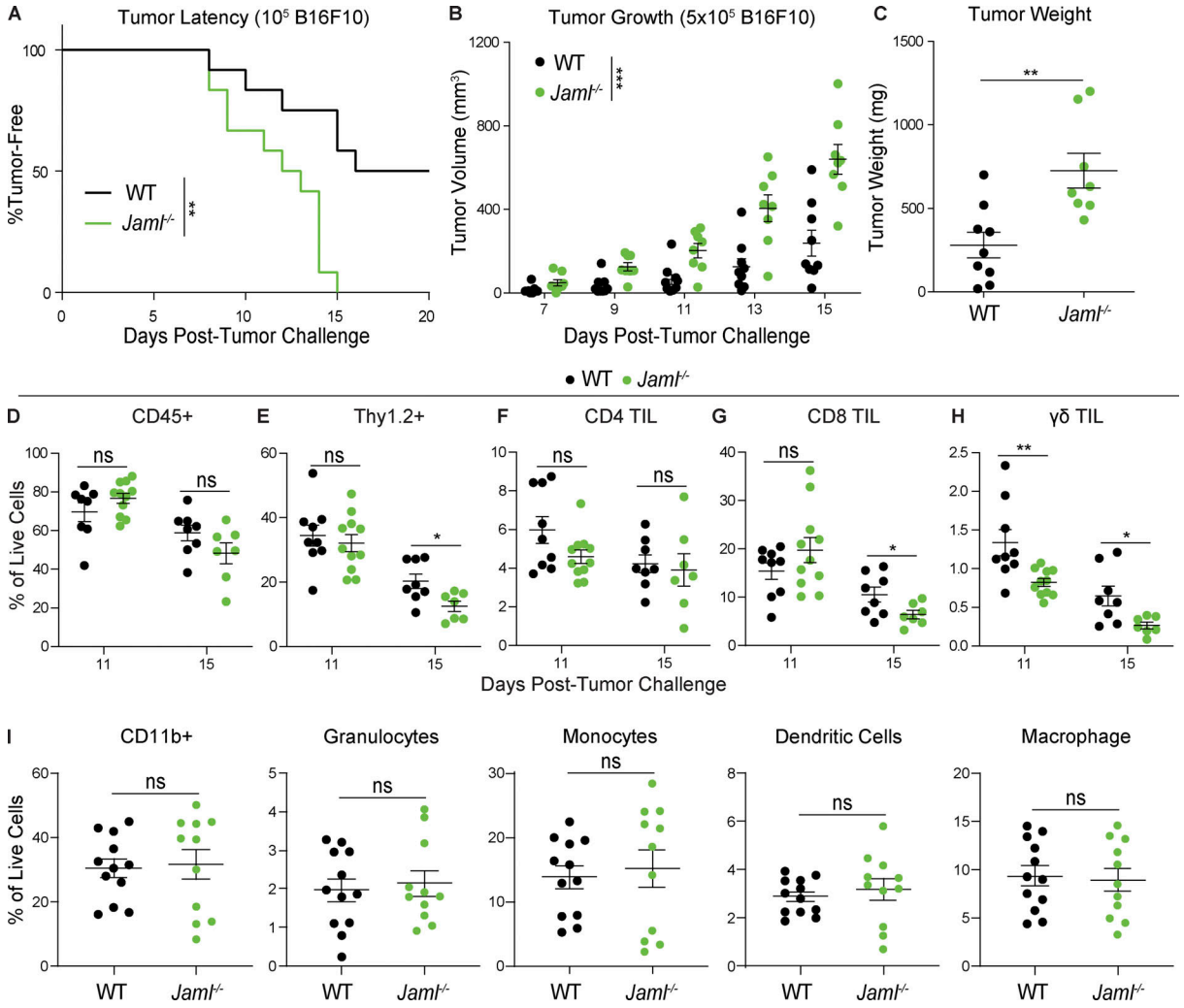

Figure 2. **JAML promotes T cell antitumor immunity against B16F10 melanoma. (A–C)** WT and *Jaml*$^{-/-}$ mice were challenged with B16F10 melanoma cells. **(A)** Kaplan-Meier plot of tumor latency following challenge with 10^5 cells (n = 12/group). **(B and C)** Tumor growth (B) and tumor weights (C) on day 15 mice after challenge with 5 × 10^5 cells (n = 8–9/group). **(D–I)** B16F10 tumor tissue was isolated from WT and *Jaml*$^{-/-}$ mice on either day 11 or day 15 after tumor challenge and analyzed by flow cytometry. Frequency of (D) CD45$^+$ cells, (E) Thy1.2$^+$ TILs, (F) CD4$^+$ TILs, (G) CD8$^+$ TILs, and (H) γδTCR$^+$ TILs. **(I)** Frequency of myeloid cell subsets on day 15. Data in A–H are expressed as mean ± SEM and are representative of at least three independent experiments; data shown represent combined analysis of two independent experiments. WT (n = 8–9), *Jaml*$^{-/-}$ (n = 7–11) in D–H; WT (n = 12), *Jaml*$^{-/-}$ (n = 11) in I. *, P < 0.05; **, P < 0.01; ***, P < 0.001 as assessed by (A) log-rank P value or (B–I) Student's t test.

Although we observed no differences in production of granzyme B (Fig. S4 B), CD8 TILs, but not CD4 TILs, in *Jaml*$^{-/-}$ mice expressed significantly more Eomes and less T-bet than CD8 TILs in WT animals (Fig. 4, B and C). Increased Eomes expression by CD8 TILs was associated with increased PD-1 expression, which resulted in a substantially larger fraction of PD-1$^+$Eomes$^+$ CD8 TILs in *Jaml*$^{-/-}$ than in WT mice (Fig. 4 D). Together, these results suggest that CD8 TILs become dysfunctional at an earlier stage of tumor growth in the absence of JAML expression but that other mechanisms of tumor immunosuppression limit JAML-CXADR–mediated antitumor immunity at later stages of tumor growth.

CXADR expression decreases during melanoma progression

Based on the role of JAML in TIL function described above and our previous work that established the function of JAML's cognate ligand, CXADR, as a self-stress molecule during cutaneous wounding (Witherden et al., 2010), we further examined CXADR expression during tumor progression, starting with B16F10 melanoma. Although B16F10 cells did not express CXADR in vitro (Fig. 5 A), CXADR expression was detected within tumor tissue on day 11 after tumor challenge as well as within adjacent normal epidermal tissue by confocal microscopy (Fig. 5 B). Analysis of *Cxadr* mRNA expression demonstrated that overall expression was significantly higher in normal mouse epidermis than in bulk B16F10 tumor tissue and that *Cxadr* expression decreased during tumor growth in vivo (Fig. 5, C and D). Additional analysis of published gene expression data (Flesher et al., 2020) revealed that normal mouse melanocytes do not express *Cxadr* (Fig. 5 E), which suggests that expression is associated with tumorigenesis.

To determine if similar patterns of CXADR dysregulation occur in human melanoma, we analyzed published human gene

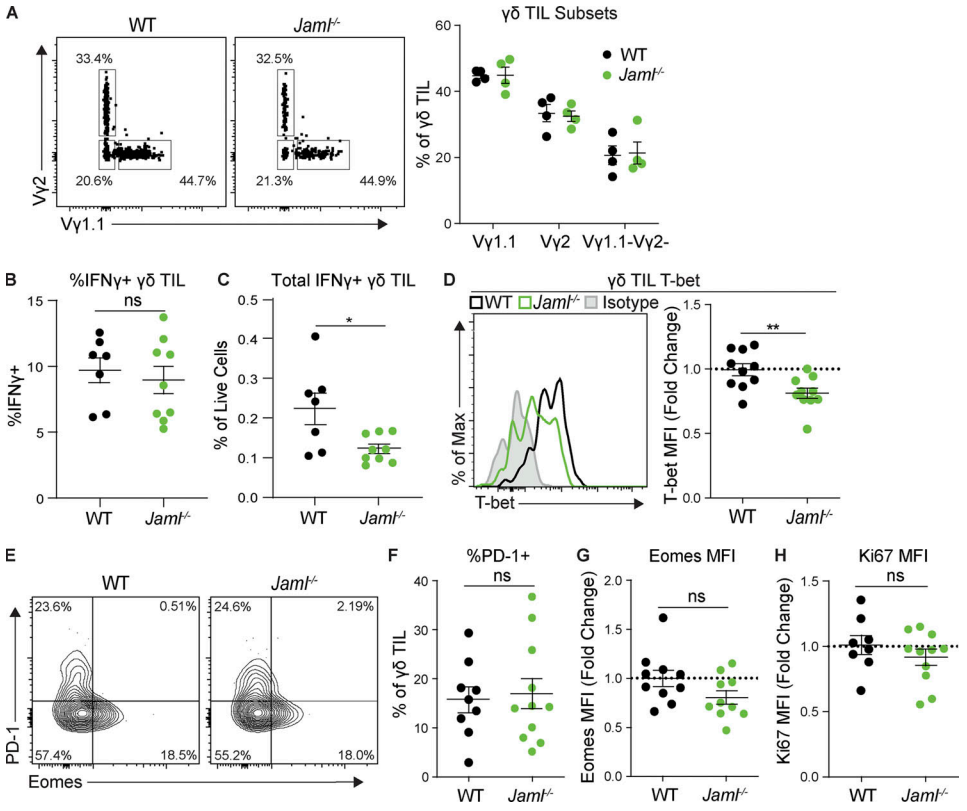

Figure 3. **JAML supports initial γδ T cell activation in response to tumor growth. (A–H)** Tumor tissue was isolated from WT and *Jaml*$^{-/-}$ mice on day 11 after B16F10 tumor challenge and analyzed by flow cytometry. **(A)** Representative flow cytometry plots of γδ TIL subsets and frequency of Vγ1.1$^+$, Vγ2$^+$, and Vγ1.1$^-$Vγ2$^-$ γδ T cells within γδTCR$^+$ TILs (n = 4/group). **(B and C)** Frequency of (B) IFNγ production by γδ TIL and (C) total IFNγ$^+$ γδ TILs (n = 7–9/group). **(D)** Representative histogram and quantification of T-bet expression by γδ TILs (fold change compared with WT mean). **(E)** Representative flow cytometry plots of γδ TIL PD-1 and Eomes expression. **(F)** Frequency of PD-1 expression by γδ TILs. **(G and H)** Quantification of (G) Eomes and (H) Ki67 MFI by γδ TIL (fold change compared with WT mean). Data in A–H are expressed as mean ± SEM and are representative of at least three independent experiments; B–H show the results of combined analysis of two independent experiments. **(B and C)** WT (n = 7) and *Jaml*$^{-/-}$ (n = 9). **(D and F–H)** WT (n = 8–10) and *Jaml*$^{-/-}$ (n = 10–11). *, P < 0.05; **, P < 0.01; Student's t test (B–H).

expression datasets. In the TCGA SKCM cohort, *CXADR* expression was decreased in metastatic lesions compared with primary samples and compared with normal skin (derived from a head and neck squamous cell carcinoma cohort; Fig. 5 F). In two additional datasets that included benign melanoma nevi (Badal et al., 2017; Talantov et al., 2005), *CXADR* was highly expressed at similar levels in both normal skin and benign melanoma nevi but was significantly decreased in primary malignant lesions and through the stages of disease (T1–T4; Fig. 5, G and H). In a third study (Hanniford et al., 2020), normal human melanocytes expressed low levels of *CXADR*, consistent with what was found for mouse melanocytes, whereas short-term cultures (STCs) of primary melanoma, but not metastatic melanoma from LN or bone marrow, expressed significantly higher levels of *CXADR* (Fig. 5 I). Together with our analysis of CXADR expression in the mouse B16F10 melanoma model, these results show that CXADR expression is low on normal melanocytes, is increased during early stages of melanoma growth, and is then progressively lost during malignant transformation and tumor growth.

JAML costimulation activates effector CD8 and γδ T cells

We previously described a noncompetitive JAML agonist antibody (HL4E10) that can be used to costimulate DETCs but not naive lymphoid CD8 and γδ T cells, consistent with their low expression of JAML (Fig. 1 D; Witherden et al., 2010). To determine the effects of JAML agonism on previously activated T cells, we activated and expanded naive CD8 and γδ T cells sorted from WT mouse splenocytes and then tested restimulation in vitro via anti-CD3 plus either anti-CD28 or anti-JAML (HL4E10) agonist antibodies. After expansion, the majority of CD8 T cells expressed JAML (Fig. 6 A). JAML costimulation of expanded CD8 T cells resulted in significant up-regulation of the T cell activation marker CD69 and increased production of TNFα and IFNγ (Fig. 6, B and C). Following expansion, JAML was also highly expressed on splenic γδ T cells (a mixture of lymphoid Vγ1.1$^+$, Vγ2$^+$, and Vγ1.1$^-$Vγ2$^-$ subsets; Fig. 6 D). JAML costimulation of expanded γδ T cells induced increased expression of CD69, TNFα, and IFNγ (Fig. 6, E and F). In agreement with a less central role of CD28 in activation of γδ T cells (Ribot et al., 2012), JAML was more effective in inducing γδ T cell activation than CD28 (Fig. 6, E and F). Collectively, these data reveal JAML's role as a costimulatory molecule for CD8 and lymphoid γδ T cell subsets after initial T cell priming.

Anti-JAML agonism in combination with PD-1 blockade limits tumor growth in vivo

Based on the above results, we next sought to determine whether the JAML–CXADR axis could be exploited therapeutically via anti-JAML agonism in vivo. To test antitumor efficacy,

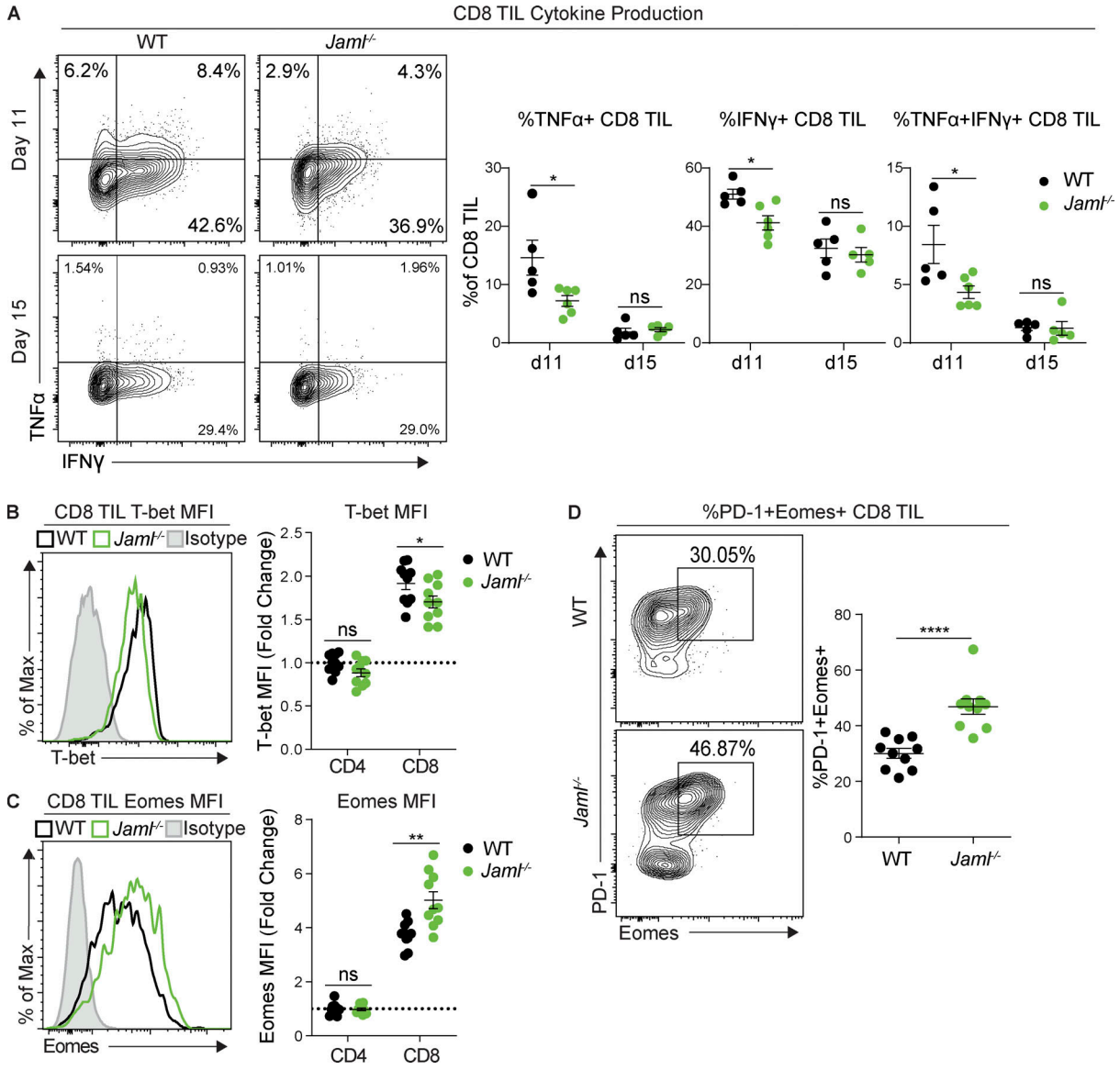

Figure 4. **CD8 T cells in *Jaml*$^{-/-}$ mice display increased markers of exhaustion within tumor tissue. (A–D)** Tumor tissue was isolated from WT and *Jaml*$^{-/-}$ mice on day 11 or 15 after B16F10 tumor challenge and analyzed by flow cytometry. **(A)** Representative flow cytometry plots and frequency of TNFα and IFNγ production by CD8 TILs on days 11 and 15 (n = 5–6/group). **(B and C)** Representative histograms and quantification of (B) T-bet and (C) Eomes MFI by CD4 and CD8 TILs (fold change compared with WT CD4 TIL mean; n = 10/group) on day 11. **(D)** Representative flow cytometry plots and frequency of PD-1^{+}Eomes^{+} CD8 TILs (n = 10/group) on day 11. Data in A–D are expressed as mean ± SEM and are representative of at least three independent experiments; B–D show the results of combined analysis of two independent experiments. *, P < 0.05; **, P < 0.01; ****, P < 0.0001; Student's t test.

we treated tumor-bearing mice with anti-JAML alone and in combination with anti–PD-1 (Fig. 7 A). Anti-JAML alone significantly slowed the growth of B16F10 tumors and extended survival (Fig. 7, B and C). On day 16 after tumor challenge, anti-JAML–treated mice had a 48.3% reduction in average tumor size compared with isotype-treated mice. In this model, anti–PD-1 treatment alone also delayed B16F10 tumor growth (Fig. 7, B and C). However, the combination of anti-JAML and anti–PD-1 resulted in a further 39.2% reduction in tumor size compared with anti–PD-1 alone by day 19 after tumor challenge and led to a significant improvement in survival in this model (Fig. 7, B and C).

To confirm that findings were not specific to the B16F10 melanoma model, we tested anti-JAML treatment in the heterotopic MC38 colon adenocarcinoma model. As with B16F10 melanoma, a high percentage (70–80%) of both CD8 and γδ TILs, but not CD4 TILs, in MC38 tumors expressed JAML (Fig. 7 D). Mice were treated with anti-JAML alone and in combination with anti–PD-1 following intradermal injection of MC38 tumor cells (Fig. 7 A). Unlike B16F10 melanoma, MC38 tumors did not exhibit a significant response to anti-JAML treatment alone with no decrease in tumor size or improved animal survival following treatment (Fig. 7, E and F). We additionally found that expression of CXADR was significantly increased in bulk MC38 tumor tissue compared with B16F10 tumor tissue following isolation on day 15 after tumor challenge (Fig. S5 A), which may limit the sensitivity to JAML agonism. MC38 tumors were sensitive to

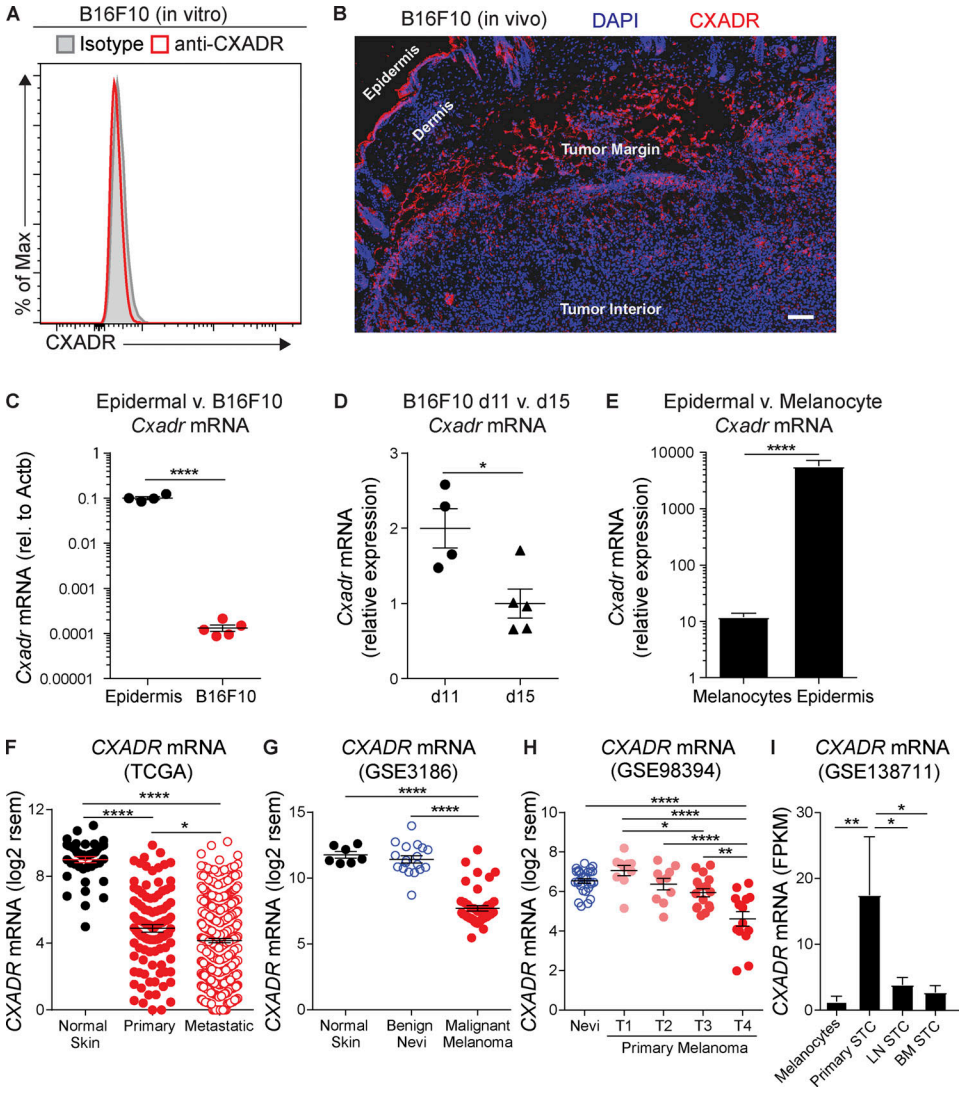

Figure 5. **CXADR expression decreases during progression of both mouse and human melanoma. (A)** B16F10 melanoma cells were cultured in vitro and analyzed by flow cytometry. Representative histogram of CXADR expression. **(B)** B16F10 tumor tissue was isolated from WT mice on day 11 tumor challenge, processed, and imaged by confocal microscopy. Representative image of CXADR (red) and DAPI (blue) staining; scale bar = 100 µm. **(C and D)** mRNA was isolated from epidermal and B16F10 tumor tissue in WT mice and analyzed by quantitative PCR. *Cxadr* mRNA expression in (C) mouse epidermis (n = 4) versus bulk B16F10 tumor tissue (n = 5) on day 15 after tumor challenge and (D) bulk B16F10 tumor tissue on day 11 (n = 4) versus day 15 (n = 5) after tumor challenge. **(E–I)** Expression of CXADR was analyzed in publicly available gene expression datasets. **(E)** *Cxadr* mRNA expression by mouse melanocytes and epidermal tissue in GEO accession no. GSE138538 (n = 4/group). **(F)** *CXADR* mRNA expression in TCGA datasets; normal skin (head and neck squamous cell carcinoma; n = 44), primary melanoma (SKCM; n = 103), malignant melanoma (SKCM; n = 366). **(G)** *CXADR* mRNA expression in GEO accession no. GSE3186 dataset; normal skin (n = 7), benign nevi (n = 18), malignant melanoma (n = 45). **(H)** *CXADR* mRNA expression in GEO accession no. GSE98394 dataset; benign nevi (n = 27), primary T1 (n = 10), T2 (n = 10), T3 (n = 16), T4 (n = 14) melanoma. **(I)** *CXADR* mRNA expression in GEO accession no. GSE138711 dataset; melanocytes (n = 5), primary STC (n = 3), LN STC (n = 5), bone marrow (BM) STC (n = 5). Data in A–D are representative of at least two independent experiments. Data in C–I are expressed as mean ± SEM. *, P < 0.05; **, P < 0.01; ****, P < 0.0001; Student's t test (C–E) and ANOVA with post hoc Tukey's test (F–I).

anti–PD-1 treatment, reducing tumor volume and improving overall survival, consistent with previous reports (Fig. 7, E and F; Juneja et al., 2017). However, the combination of anti-JAML and anti–PD-1 resulted in significant reduction in tumor growth compared with anti–PD-1 alone, although this did not lead to a significant difference in median survival (Fig. 7, E and F). These results suggest that JAML agonism can improve the efficacy of PD-1 blockade in multiple tumor models in a manner that is not strictly dependent on CXADR expression within the TME.

Anti-JAML therapy modulates intratumoral CD8 and γδ T cells

To investigate the effects of anti-JAML treatment on TILs in vivo, we challenged WT mice with B16F10 melanoma, treated mice with either isotype IgG or anti-JAML antibodies on day 7 after tumor challenge, and then profiled TIL numbers and activation 5 d later, on day 12 after tumor challenge. At this time point, anti-JAML treatment did not alter CD4, CD8, or γδ TIL numbers or ex vivo cytokine production (Fig. S5, B–F). However, in anti-JAML–treated mice, a higher percentage of γδ TILs expressed the activation marker CD69 (Fig. 7 G), consistent with

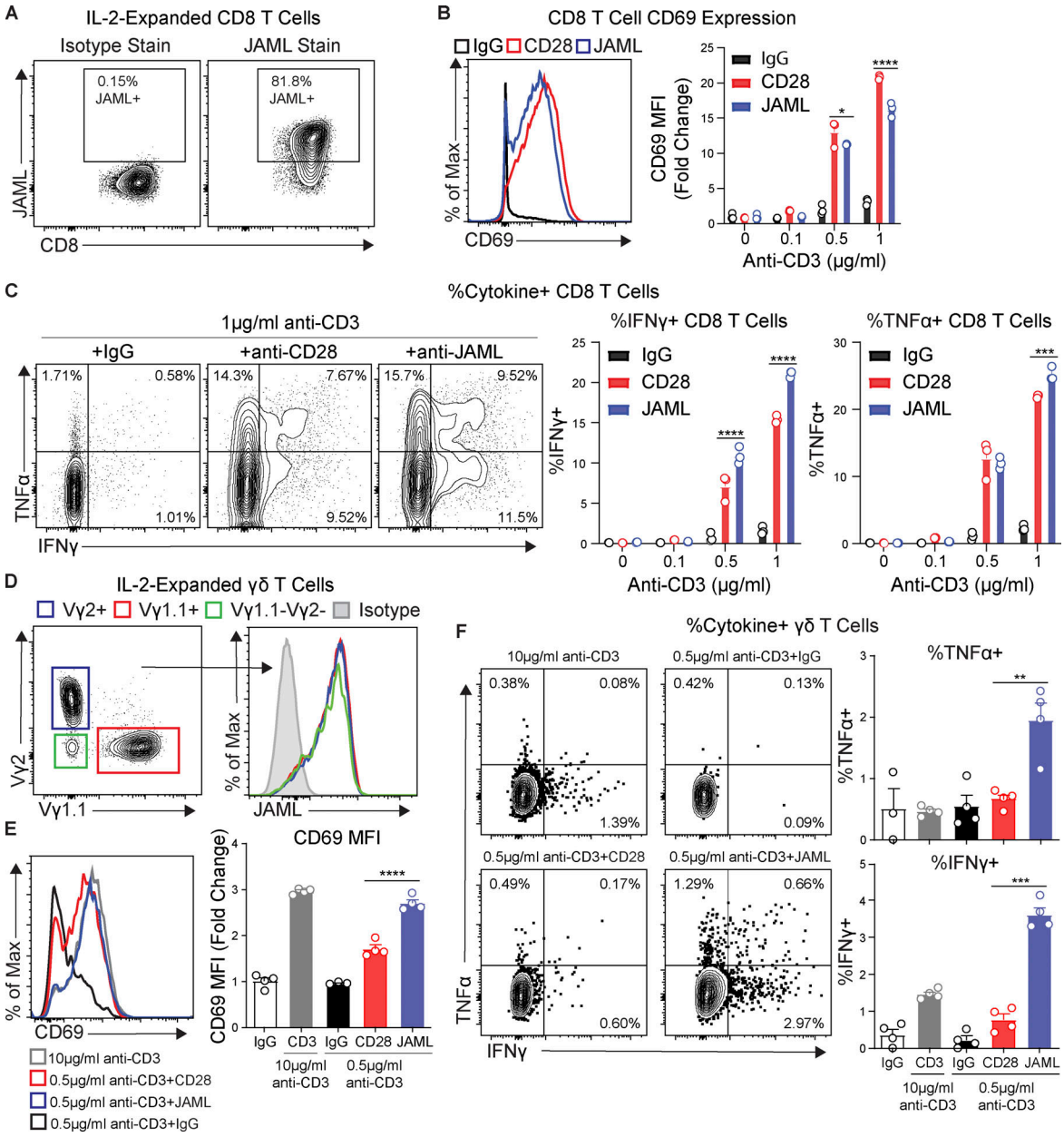

Figure 6. **JAML costimulation activates effector CD8 and γδ T cells. (A–E)** CD8 and γδ T cells from WT mice were expanded ex vivo and then analyzed by flow cytometry before and after overnight costimulation via CD28 or JAML. **(A)** Representative flow cytometry plots of JAML expression by expanded CD8 T cells before costimulation. **(B)** Representative histogram and quantification of CD69 MFI (fold change compared with unstimulated condition) by CD8 T cells after costimulation. **(C)** Representative flow cytometry plots and frequency of TNFα and IFNγ production by expanded CD8 T cells after costimulation. **(D)** Representative histogram of JAML expression by expanded γδ T cells. **(E)** Representative histogram and quantification of CD69 MFI (fold change compared with unstimulated condition) by γδ T cells after costimulation. **(F)** Representative flow cytometry plots and frequency of TNFα and IFNγ production by expanded γδ T cells after costimulation. Data are expressed as mean ± SEM and are representative of three independent experiments. **(B and C)** *n* = 3 replicates per condition. **(E and F)** *n* = 3–4 replicates per condition. *, P < 0.05; **, P < 0.01; ***, P < 0.001; ****, P < 0.0001; ANOVA with post hoc Tukey's test (B, C, E, and F).

the effects of JAML costimulation on effector γδ T cells in vitro. A similar increase in CD69 expression was not observed on CD8 TILs in anti-JAML–treated mice (Fig. S5 G). However, a lower frequency of CD8 TILs in anti-JAML–treated mice displayed a dysfunctional phenotype measured by coexpression PD-1 and Eomes (Fig. 7 H). Together, these results suggest that anti-JAML agonism increases the activity of both CD8 and γδ TILs, resulting in improved control of tumor growth.

The antitumor effect of anti-JAML agonism is target dependent and requires the presence of both CD8 and γδ T cells

To confirm on-target engagement of host immune cells in vivo, we tested the antitumor efficacy of anti-JAML in WT versus *Jaml*$^{-/-}$ mice. As anticipated, tumor growth in WT mice treated with anti-JAML was reduced compared with WT mice treated with isotype IgG antibody. However, this antitumor effect was

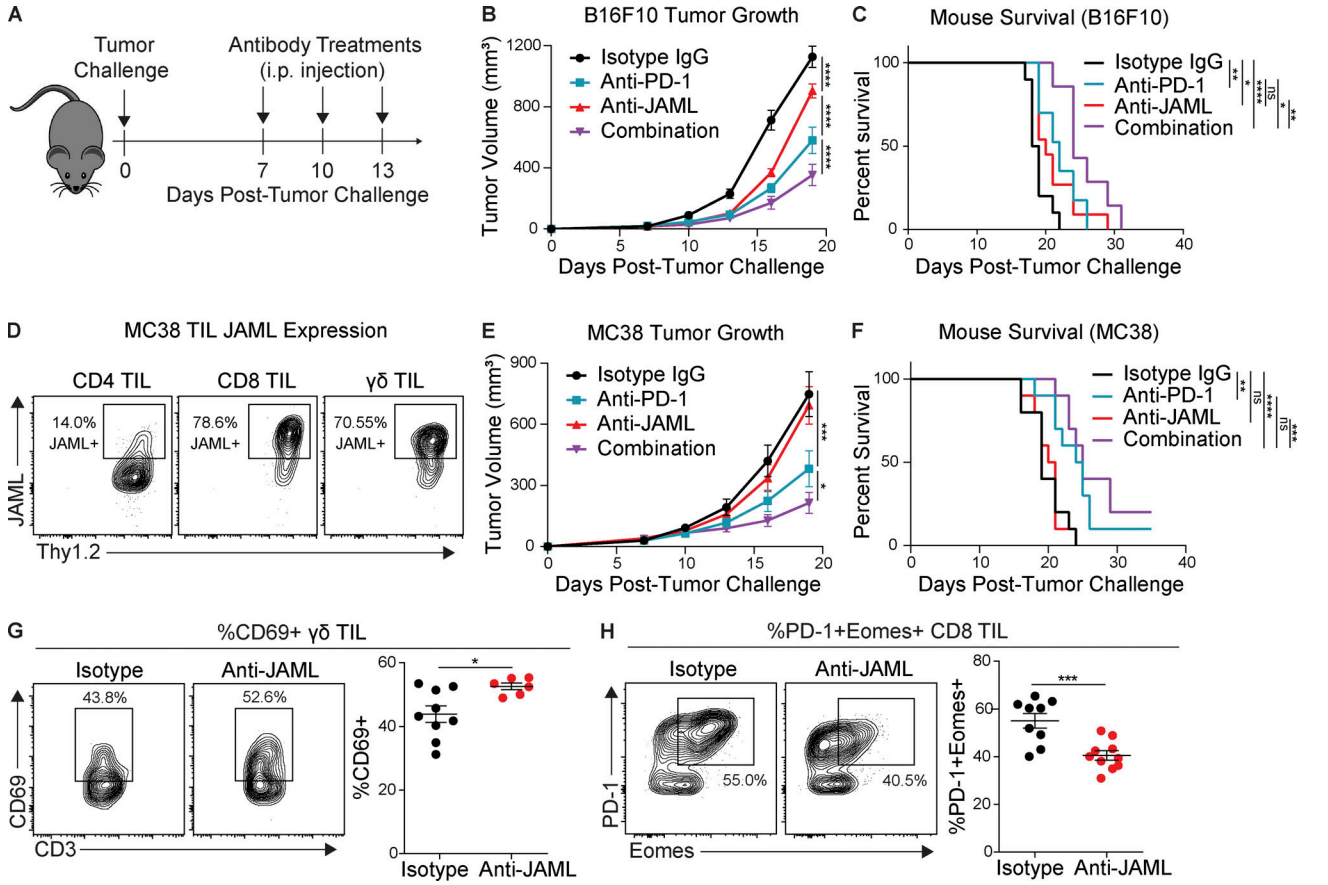

Figure 7. **Anti-JAML agonism in combination with PD-1 blockade limits tumor growth in vivo. (A–C)** WT mice were challenged with B16F10 melanoma and treated with isotype IgG, anti-JAML, anti–PD-1, or anti–PD-1 plus anti-JAML antibodies (combination) antibodies. **(A)** Timing of antibody treatments. **(B and C)** (B) Tumor growth and (C) mouse survival (n = 8–11/group). **(D)** MC38 tumor tissue isolated from WT mice on day 15 after tumor challenge was analyzed by flow cytometry. Representative flow cytometry plots of JAML expression by CD4, CD8, and γδ TILs. **(E and F)** WT mice were challenged with MC38 colon adenocarcinoma and then treated and monitored as in B and C. (E) Tumor growth and (F) mouse survival (n = 10/group). **(G and H)** Mice were challenged with B16F10 melanoma and treated with isotype IgG or anti-JAML antibodies on day 7 after tumor challenge. Tumor tissue was isolated and analyzed by flow cytometry on day 12. Representative flow cytometry plots and frequency of (G) γδ TIL CD69 (n = 6–9/group) and (H) PD-1⁺Eomes⁺ CD8 TILs (n = 9–10/group). Data in B–H are expressed as mean ± SEM and represent a combined analysis of two (D–H) or three (B and C) independent experiments. *, P < 0.05; **, P < 0.01; ***, P < 0.001; ****, P < 0.0001 as assessed by (B and E) ANOVA with post hoc Tukey's test, (C and F) Kaplan-Meier log-rank P value, or (G and H) Student's t test.

completely lost in *Jaml*$^{-/-}$ mice, which confirms that the effect of anti-JAML treatment is mediated through host immune cells and excludes any possible interactions with tumor cells or nonspecific effects of antibody treatment (Fig. 8, A and B).

We next sought to address the contribution of both CD8 and γδ T cells to the effect of anti-JAML treatment in vivo. To test the impact of γδ T cells on the antitumor effect of anti-JAML in vivo, we challenged WT and *Tcrd*$^{-/-}$ C57BL/6J mice with B16F10 melanoma and treated each group with either isotype IgG or anti-JAML antibodies (Fig. 7 A). Strikingly, the antitumor efficacy of anti-JAML treatment observed in WT mice was not seen in *Tcrd*$^{-/-}$ mice, demonstrating that γδ T cells are required for the antitumor effects of anti-JAML treatment (Fig. 8, C and D). To assess the contribution of CD8 T cells, we treated WT mice with either isotype IgG or depleting anti-CD8 antibodies starting on day 4 after tumor challenge and then concurrently with isotype IgG or anti-JAML antibodies on days 7, 10, and 13. Depletion of CD8 T cells was confirmed by flow cytometric analysis of peripheral blood T cells collected on day 11 (Fig. S5 H). The effect of anti-JAML treatment was abrogated in the CD8 T cell–depleted mice compared with the nondepleted animals (Fig. 8, E and F). These results demonstrate that the antitumor effect of anti-JAML agonism is dependent on the presence of both CD8 and γδ T cells in vivo.

Discussion

To date, the focus of cancer immunotherapy has centered on reversal of T cell dysfunction and the role of inhibitory receptors within the TME (Thommen and Schumacher, 2018). Equally important, however, is the elucidation of mechanisms required to promote and sustain TIL activity within the context of an immunosuppressive TME. In our previous work, we identified JAML–CXADR interactions as a unique costimulatory mechanism that controls activation of tissue-resident γδ T cells in the context of wound healing (Witherden et al., 2010). Given the

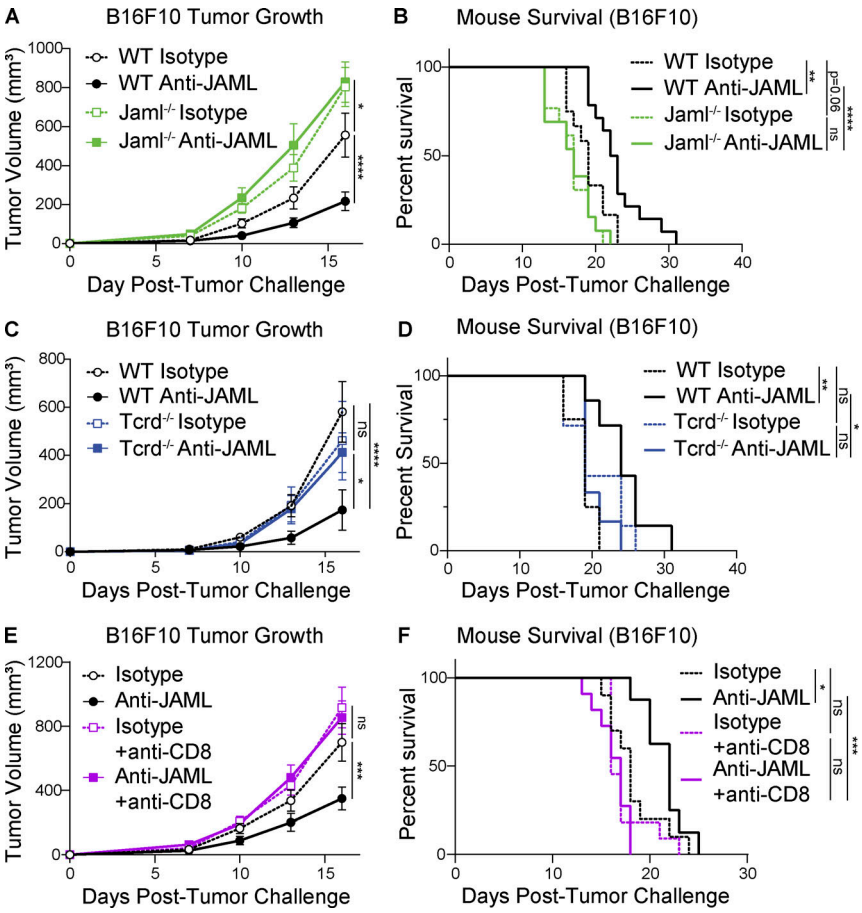

Figure 8. **The antitumor effect of anti-JAML agonism is target dependent and requires the presence of both CD8 and γδ T cells. (A–F)** Mice were challenged with B16F10 melanoma and treated with isotype IgG or anti-JAML antibodies on days 7, 10, and 13 after tumor challenge. **(A and B)** (A) Tumor growth in and (B) survival of WT versus *Jaml*$^{-/-}$ mice (n = 11–15/group). **(C and D)** (C) Tumor growth in and (D) survival of WT versus *Tcrd*$^{-/-}$ mice (n = 6–8/group). **(E and F)** (E) Tumor growth in and (F) survival of WT mice with or without CD8 T cell depletion (n = 9–11/group). Data in A–F represents a combined analysis of two independent experiments. Data in A, C, and E are expressed as mean ± SEM. *, P < 0.05; **, P < 0.01; ***, P < 0.001; ****, P < 0.0001; (A, C, and E) ANOVA with post hoc Tukey's test or (B, D, and F) Kaplan-Meier log-rank P value.

important roles of γδ T cells in antitumor immunity and evidence that JAML–CXADR interactions may also be important for CD8 T cell and myeloid cell responses (Luissint et al., 2008; Guo et al., 2009), we sought to define the role of JAML–CXADR interactions in antitumor immunity.

Initial analysis of human cancer gene expression datasets revealed that high expression of JAML was a favorable prognostic factor in certain cancer types, most notably head and neck, lung, and melanoma, and for response to anti–PD-1 in the context of metastatic melanoma. To identify roles of JAML–CXADR interactions within the TME, we used the mouse B16F10 melanoma model and found that a large fraction of both CD8 and γδ TILs expressed JAML, whereas expression on resting lymphoid subsets was significantly lower. In vitro, we demonstrated that naive CD8 and γδ T cells up-regulate JAML shortly after activation and can then be further activated by JAML costimulation. These data suggest that JAML is an important activation molecule for effector CD8 and γδ T cell responses after initial T cell priming and infiltration into the TME. In support of this hypothesis, *Jaml*$^{-/-}$ mice were more susceptible to tumor formation and had accelerated B16F10 melanoma growth compared with WT mice, which was associated with decreased levels of activation in γδ TILs and increased markers of CD8 TIL dysfunction. Although JAML is also expressed by myeloid cell subsets, most notably on intratumoral DCs, JAML knockout does not appear to impact myeloid cell infiltration or persistence in the TME. Based on these results, we focused our investigation on the impact of JAML–CXADR interactions in antitumor immunity on CD8 and γδ T cells.

Tissue-resident γδ T cells constitutively express JAML, and signaling via interactions with CXADR is a primary mechanism of activation (Witherden et al., 2010). We previously found that resting lymphoid γδ T cells do not respond to JAML costimulation, but other potential roles of JAML on these subsets were not examined (Witherden et al., 2010). Here we found that lymphoid γδ T cell subsets, but not DETCs, infiltrated into B16F10 melanoma tumors and that accumulation of these subsets within the TME was impaired in *Jaml*$^{-/-}$ mice. Furthermore, γδ TILs in *Jaml*$^{-/-}$ mice displayed lower levels of activation, as assessed by decreased numbers of IFNγ-producing cells and reduced T-bet expression compared with WT mice. In contrast to CD8 TILs, this defect in γδ TIL activation was not associated with changes in PD-1 or Eomes expression. Additionally, similar expression of the proliferation marker Ki67 by γδ TILs in WT and *Jaml*$^{-/-}$ mice at an early stage of tumor growth supports the notion that JAML is more important for initial γδ T cell activation and tumor infiltration than proliferation and survival within the TME. Together with in vitro costimulation via JAML, these data suggest that JAML is also an important costimulatory signal to lymphoid γδ T cells.

Prior studies have reported JAML expression on human memory (CD45RO^{+}) CD8 T cells in peripheral blood (Luissint et al., 2008) and, more recently, by CD8 TILs of both human lung cancer and head and neck cancer in single-cell RNA-sequencing

studies (Clarke et al., 2019; Yost et al., 2019). However, a role for JAML–CXADR interactions in mediating CD8 T cell responses has not been characterized. In the B16F10 tumor model, initial CD8 T cell infiltration was not reduced in *Jaml*$^{-/-}$ mice compared with WT mice, which suggests that JAML–CXADR interactions are not critical for CD8 TIL tumor homing. However, at an early stage of tumor growth (day 11), *Jaml*$^{-/-}$ CD8 TILs displayed markers of increased T cell dysfunction, as assessed by increased expression of PD-1 and Eomes with decreased levels of T-bet, TNFα, and IFNγ compared with WT CD8 TILs. Consistent with this impaired phenotype, CD8 TIL numbers in *Jaml*$^{-/-}$ mice were reduced compared with WT mice at a later stage of tumor growth. By this later time point (day 15), CD8 TIL cytokine production was similar in WT and *Jaml*$^{-/-}$ mice, which may be due to decreased CXADR expression observed during tumor progression or other mechanisms that limit JAML-CXADR–mediated antitumor immunity. These data, together with the ability to induce effector CD8 T cell activation via JAML costimulation in vitro, strongly support the notion that direct JAML signals are important for CD8 TIL responses in vivo.

CXADR has been studied as a target for adenovirus-based gene therapy in human cancers (Bergelson et al., 1997; Li et al., 1999b; Li et al., 1999a), but only a small number of studies have outlined specific functions in the context of tumor growth and progression. Loss of CXADR expression has been associated with increased growth of human bladder cancer, an increased rate of gastric cancer metastasis, and epithelial–mesenchymal transition in breast cancer (Matsumoto et al., 2005; Lacher et al., 2006; Anders et al., 2009; Nilchian et al., 2019). However, potential roles of CXADR expression in melanoma development and progression have not been characterized. In both mouse and human melanoma, we found evidence that CXADR expression is higher during early stages of tumor growth than on normal melanocytes. These data suggest that, as in the context of epithelial wound healing (Witherden et al., 2010), CXADR may act as a tissue stress signal to promote immune responses. However, CXADR expression significantly decreases as melanoma lesions progress, which may limit immune responses within the TME and allow increased tumor growth. Although CXADR expression was not associated with response to PD-1 blockade in a small cohort of patients with metastatic melanoma, these findings highlight the need for further investigation into the impact of CXADR down-regulation on antitumor immunity and response to immunotherapy during tumor progression.

Although the loss of CXADR expression with increased malignancy in human melanoma samples is striking, this phenomenon does not appear to be generalizable to all cancer types. In a separate study that analyzed both normal and malignant tissues, CXADR expression was increased in certain cancers, such as lung, cervical, and basal cell cancers, but was decreased in others, such as colon, prostate, and kidney cancers, compared with normal tissues (Reeh et al., 2013). Additionally, other studies have reported both increased and decreased expression of CXADR in response to cytokines such as TNFα, IFNγ, and TGFβ (Nilchian et al., 2019; Vincent et al., 2004; Zussy et al., 2016; Ito et al., 2000). Together, these data suggest that regulation of CXADR expression is highly context dependent and likely dependent on the cancer type and tissue of origin.

In the B16F10 melanoma tumor model, treatment with an agonist anti-JAML antibody limits tumor growth and potentiates the efficacy of anti–PD-1 blockade. Furthermore, anti-JAML treatment improves the efficacy of anti–PD-1 in the more immunogenic MC38 tumor model (Juneja et al., 2017). Mechanistically, we show that anti-JAML treatment is associated with markers of increased γδ TIL activation and reduced CD8 TIL dysfunction. To determine the dependence of anti-JAML treatment on both CD8 and γδ T cells, we used antibody-mediated CD8 T cell depletion and *Tcrd*$^{-/-}$ mice, respectively. Notably, we show that the presence of both CD8 and γδ T cells is required for the antitumor efficacy of anti-JAML treatment in the B16F10 model. The loss of anti-JAML antitumor efficacy upon CD8 T cell depletion clearly demonstrates that CD8 T cells are required to mediate anti-JAML–induced antitumor immunity. Additionally, loss of γδ T cells also results in a defective antitumor immune response that cannot be rescued by anti-JAML treatment, which is consistent with previous data that demonstrated CD8 TIL dysfunction in the absence of γδ T cells (Gao et al., 2003). Based on the known antitumor functions of γδ T cells in a variety of tumor models and the central role of CD8 T cells in response to immunotherapies (Girardi et al., 2001; Gao et al., 2003; Silva-Santos et al., 2019), we expect that that the presence of both CD8 and γδ T cells is also required for the additive effect of anti-JAML treatment in combination with PD-1 blockade in the MC38 tumor model. Together with the ability to costimulate effector CD8 and γδ T cells via JAML in vitro, these results suggest that CD8 and γδ TIL are targets of JAML agonism in vivo. However, additional work is needed to determine whether JAML agonism results in sequential or concurrent activation of CD8 and γδ T cells and if myeloid cells are also a relevant target within the TME.

Agonism of T cell costimulatory molecules is a promising approach for cancer immunotherapy. Other T cell agonist therapies currently in clinical evaluation include targeting the B7-CD28 family members CD28 and inducible T cell costimulator as well as TNF receptor superfamily molecules such as 4-1BB, OX40, CD40L, and CD27 (Mayes et al., 2018). The addition of costimulatory molecule signaling motifs to the intracellular domains of chimeric antigen receptor T cells further underscores their importance in maintaining an effective T cell–mediated antitumor response (Schultz and Mackall, 2019; Mayes et al., 2018). JAML agonism may prove to be a novel approach to provide T cell costimulation. Indeed, though JAML has classically been studied as a junctional adhesion molecule, it shares homology with the CD28 intracellular signaling domain, which contains a PI3K binding motif YMxM, supportive of its role as a costimulatory molecule (Verdino et al., 2010).

Here we demonstrate that JAML–CXADR interactions are a novel component of antitumor immunity that supports the function of both CD8 and γδ TIL, and, correspondingly, this may support a mechanism for why decreased CXADR expression within melanoma correlates with increased malignancy. Importantly, treatment with an agonist anti-JAML antibody can increase activation of CD8 and γδ TILs, afford significant decreases in tumor burden, and improve responses of tumors to anti–PD-1 blockade. Overall, these findings highlight an important role of JAML–CXADR interactions in antitumor

immunity and identify JAML as a target for improved cancer immunotherapy.

Materials and methods

Mice

C57BL/6J WT mice were obtained from the rodent breeding colony at The Scripps Research Institute (TSRI). *Jaml*$^{-/-}$ mice were obtained from Eli Lilly (project T3889 KO; line 3492), and *Tcrd*$^{-/-}$ mice were obtained from The Jackson Laboratory. Strains were maintained under standard specific-pathogen-free TSRI vivarium conditions. Mice were used for experiments at 8–10 wk of age. All procedures were approved by the TSRI Institutional Animal Care and Use Committee.

Mouse tumor models

B16F10 melanoma cells were kindly provided by Dr. Linda Sherman (TSRI, La Jolla, CA). MC38 cells were kindly provided by Dr. John Teijaro (TSRI, La Jolla, CA). Tumor cells were grown in complete DMEM (Invitrogen) supplemented with 10% heat-inactivated FCS. For tumor challenge studies, mice were shaved 24–48 h before tumor injection. For tumor cell injections, cells were detached using 0.05% trypsin-EDTA (Invitrogen), washed, and suspended in 1× Dulbecco's PBS (DPBS). Cells were then injected intradermally with a 1-ml syringe and a 25-gauge needle in a total volume of 100 µl. To determine tumor latency, mice were injected with 10^5 B16F10 melanoma cells and assessed daily for palpable tumors. To measure tumor growth rates, mice were injected with either 5×10^5 B16F10 or 2×10^5 MC38 cells. After tumor formation, tumor growth was measured using calipers every 2–3 d. Tumors were measured in two directions along the long (D) and short (d) axes in order to calculate tumor volume ($0.5 \times D \times d^2$). Mouse survival was tracked until tumors grew to 1,200 mm^3 in size. Mice that developed severe tumor ulceration or cachexia during experiments were euthanized. For in vivo antibody treatments, mice were treated with low-endotoxin, functional grade anti-JAML (clone HL4E10; Verdino et al., 2011; produced at the Scripps California Institute for Biomedical Research), anti–PD-1 (clone RMP1-14; Leinco), rat IgG2a isotype (clone 1-1; Leinco), or Armenian hamster IgG (clone PIP; Leinco) antibodies. 200 µg of each antibody was diluted in 1× DPBS and administered via i.p. injection in a total volume of 200 µl. Antibodies were administered on days 7, 10, and 13 after tumor challenge for tumor growth studies and on day 7 for analysis of TILs by flow cytometry. For CD8 T cell depletion studies, mice were treated with 200 µg anti-CD8 (clone YTS-169; Leinco) or rat IgG2a isotype (clone 1-1; Leinco) antibodies starting on day 4 after tumor challenge and then concurrently with Armenian hamster IgG or anti-JAML antibodies on days 7, 10, and 13 after tumor challenge.

Tissue processing and flow cytometry

B16F10 tumor tissue was isolated from mouse skin, and surrounding epidermal and dermal skin tissue was removed using a scalpel. Tumors were weighed and then briefly minced and digested in RPMI 1640 medium (Invitrogen) supplemented with 0.5 mg/ml collagenase type IV (Fisher Scientific), 0.1 mg/ml DNase I (Sigma-Aldrich), and 1 mg/ml trypsin inhibitor (Sigma-Aldrich) at 37°C with shaking for 45 min. Samples were then filtered through 70-µm mesh strainers, washed in 1× PBS, and treated with 1× RBC lysis buffer (BioLegend). The spleen and LNs were dissociated through 70-µm mesh strainers. Spleen samples were additionally treated with 1× RBC lysis buffer. For ex vivo restimulation for cytokine detection, samples were plated in 96-well round-bottomed plates (Thermo Fisher Scientific) at a concentration of 2×10^6 cells per well in complete RPMI medium supplemented with 10% FCS, 50 ng/ml PMA (Sigma-Aldrich), 500 ng/ml ionomycin (Sigma-Aldrich), and 4 µg/ml monensin (Sigma-Aldrich) for 4 h at 37°C. Cells were stained with conjugated antibodies in 1× DPBS supplemented with 2% FCS and 0.05% sodium azide (Fisher Scientific). For intracellular staining of cytokines and transcription factors, cells were fixed and permeabilized using BD Cytofix/Cytoperm or eBioscience Foxp3/transcription factor staining kits. Stained cells were quantified by flow cytometry on LSR II (BD Biosciences) or Aurora (Cytek) analyzers (TSRI Flow Cytometry Core). Flow cytometric data were analyzed using FlowJo software (BD Biosciences).

Flow cytometry antibodies

B16F10 cells grown in vitro were stained with unconjugated rat anti-mouse CXADR (provided by Dr. Luc Teyton, TSRI, La Jolla, CA) followed by fluorescein-conjugated rabbit anti-rat IgG secondary antibody (Vector Laboratories). The following fluorescently conjugated primary antibodies were purchased from BioLegend: antibodies against mouse CD3ε (clone 145-2C11; PerCpCy5.5), CD4 (clone GK1.5; PerCpCy5.5, Pacific Blue [PB]), CD8 (clone 53-6.7; allophycocyanin [APC], Brilliant Violet (BV) 605, PE-Cy7), CD11b (clone M1/70; BV421), CD11c (clone N418; APC), CD44 (clone IM7; FITC), CD45 (clone 30-F11; BV605), CD62L (clone MEL-14; BV605), CD69 (clone H1.2F3; FITC, BV605), F4/80 (clone BM8; PE-Cy7), γδTCR (clone GL3; BV605, FITC, PE-Cy7), IFNγ (clone XMG1.2; PE), IL-17A (clone TC11-18H10.1; PerCpCy5.5), JAML (clone HL4E10; Alexa Fluor 647), Ki67 (clone 16A8; PE), Ly6C (clone HK1.4; FITC), Ly6G (clone 1A8; PerCpCy5.5), MHCII (I-A/I-E; clone M5/114.15.2; PE), PD-1 (clone 29F.1A12; PerCpCy5.5), T-bet (clone 4B10; APC), TCRβ (clone H57-597; PB), Thy1.2 (clone 30-H12; PB, PE-Cy7), TNFα (clone MP6-XT22; APC, BV421), Vγ1.1 (clone 2.11; PE), and Vγ2 (clone UC3-10A6; FITC, APC). Antibodies against mouse Eomes (clone Dan11-mag; PE) and granzyme B (clone GB11; FITC) were purchased from Invitrogen and BD Biosciences, respectively. Fixable viability dye (eFluor 780) was purchased from eBioscience.

Tumor section imaging

B16F10 tumors were processed and stained for imaging as previously described (Rashidian et al., 2019). Briefly, tumors were fixed in 4% paraformaldehyde overnight and then dehydrated in a 30% solution of sucrose dissolved in 1× DPBS for 48 h. Tumors were then frozen in optimal cutting temperature media (VWR) on dry ice. Tissue was sectioned at 14 µm onto slides and then fixed in acetone at −20°C for 20 min. Slides were washed with 1× DPBS and blocked with 2% FCS for 1 h. Tissue was then stained with a 1:50 dilution of primary unconjugated anti-CXADR (clone H-300, 200 µg/ml; Santa Cruz Biotechnology) or an equivalent amount of polyclonal rabbit IgG isotype control (BioLegend)

antibodies for 1 h followed by staining with a 1:1,000 dilution of goat anti-rabbit Alexa Fluor 555 secondary antibody (Abcam) and a 1:1,000 dilution of DAPI (1 mg/ml stock). Slides were imaged using a Zeiss LSM 780 confocal laser scanning microscope (TSRI Microscopy Core), and images were processed using Imaris software (Oxford Instruments).

RNA isolation and quantitative PCR

Skin and tumor tissue were briefly minced in 1.7-ml Eppendorf tubes and then lysed in TRIzol reagent (Thermo Fisher Scientific). RNA was isolated from the aqueous phase after phenol-chloroform extraction. cDNA was generated using SuperScript III reverse transcription (Thermo Fisher Scientific) with random hexamers. mRNA transcripts were quantified via quantitative PCR using SYBR Green Master Mix (Bio-Rad Laboratories) and normalized to β-actin. Primer sequences were as follows: *Actb*: forward, 5′-GATCTGGCACCACACCTTCT-3′ and reverse, 5′-GGGGTG TTGAAGGTCTCAAA-3′; *Cxadr*: forward, 5′-AATGGCTGATATCCC CGTCT-3′, and reverse, 5′-ATAGATGCGTCGCCAGACTT-3′.

Gene expression analysis

Patient survival data across all TCGA cohorts were generated using the Tumor Immune Estimation Resource website (https://cistrome.shinyapps.io/timer/; Li et al., 2016). Additional analysis of gene expression in the SKCM TCGA cohort was performed by downloading data with the TCGA2STAT R package (https://rdrr.io/cran/TCGA2STAT/). Survival z-scores were obtained from the PRECOG database (https://precog.stanford.edu/). GSE3186, GSE98394 GSE138711, GSE47045, and GSE138538 gene expression datasets were downloaded from the National Center for Biotechnology Information Gene Expression Omnibus (GEO) website. Datasets were analyzed in R.

In vitro expansion of CD8 and γδ T cells

CD8 and γδ T cell splenocytes were sorted on a Sony MA900 chip cuvette sorter into RPMIc supplemented with 20% FCS. Sorted splenic CD8 T cells were expanded in vitro with anti-CD3 plus anti-CD28 for 48 h, followed by additional culturing with IL-2 for 72 h. Briefly, 6-well, flat-bottomed tissue culture plates were incubated with 50 µg/well goat anti-hamster IgG (Thermo Fisher Scientific) for 2 h at 37°C. Wells were then washed twice with RPMIc with 10% FCS added. 2×10^6 CD8 T cells were plated in each well with 1 µg/ml soluble hamster anti-mouse CD3 (clone 500A2) and 1 µg/ml anti-CD28 (clone 37.51). CD8 T cells were activated at 37°C for 48 h and then transferred into RPMIc with 10% FCS and 100 U/ml IL-2 added for an additional 72 h. To expand sorted splenic γδ T cells in vitro, 96-well, flat-bottomed tissue culture plates were incubated with 10 µg/ml anti-γδ TCR (clone GL3) for 2 h at 37°C and then washed twice with RPMIc with 10% FCS added. 50,000 γδ T cells were plated in each well and incubated for 72 h at 37°C and then transferred into RPMIc supplemented with 10% FCS and 100 U/ml IL-2 for an additional 72 h.

Costimulation assays

For CD8 T cell costimulation assays, 12-well, flat-bottomed tissue culture plates were coated with a range of anti-CD3 (clone 500A2) concentrations (0, 0.1, 0.5, or 1 µg/ml) plus 10 µg/ml Armenian hamster IgG, anti-CD28 (clone 53-6.7), or anti-JAML (HL4E10) for 2 h at 37°C and then washed twice with RPMIc with 10% FCS added. For γδ T cell costimulation assays, wells were coated with 0.5 µg/ml anti-CD3 (clone 500A2) plus 10 µg/ml Armenian hamster IgG, anti-CD28 (clone 53-6.7), or anti-JAML (HL4E10) as described above. Wells coated with 10 µg/ml of Armenian hamster IgG alone were used as a negative control, and 10 µg/ml of anti-CD3 was used as a positive control for stimulation of γδ T cells. 2.5×10^5 expanded CD8 or γδ T cells (as described above) were added to coated wells for 24 h at 37°C before staining for FACS analysis. To detect cytokine production, 4 µg/ml of monensin was added to each well for the last 4 h of incubation before staining for flow cytometric analysis.

Statistics

Data shown are representative of at least two or three independent experiments. Data are pooled between experiments when applicable. Statistical analyses were performed using GraphPad Prism version 8 software. Statistical testing and associated P values are listed in the figure legends. Statistically significant data ($P < 0.05$) are noted in the figures.

Online supplemental material

Fig. S1 shows associations of CXADR expression with clinical responses to PD-1 blockade in metastatic melanoma patients, flow cytometry gating strategies for T cell and myeloid cell subsets, and characterization of JAML expression by CD8 and γδ T cells. Fig. S2 shows phenotypic analysis of splenic T cells in naive WT and *Jaml*$^{-/-}$ mice. Fig. S3 shows characterization of Ki67 expression on TILs isolated from WT and *Jaml*$^{-/-}$ mice on day 15 after tumor challenge with B16F10 melanoma. Fig. S4 shows characterization of CD4 TIL cytokine production on days 11 and 15 after B16F10 tumor challenge and CD4 and CD8 TIL granzyme B production on day 11 after B16F10 tumor challenge. Fig. S5 shows *Cxadr* mRNA expression in B16F10 versus MC38 tumor tissue, quantification of TIL subsets and cytokine production following isolation from B16F10 tumor tissue from mice treated with isotype IgG or anti-JAML antibodies, and confirmation of in vivo CD8 T cell depletion.

Data availability

Jaml$^{-/-}$ C57BL/6J mice were obtained through an MTA with Eli Lilly. All other data needed to evaluate the conclusions in the paper are presented in the paper or the online supplemental material.

Acknowledgments

We dedicate this article to the late W.L. Havran, who was a driving force for this project. We thank L. Sherman, J. Teijaro, B. Felding, members of the Young laboratory, and former members of the Havran laboratory for critical discussion and feedback related to this project. We also thank L. Sherman for B16F10 cells and J. Teijaro for MC38 cells. This is manuscript 30053 from The Scripps Research Institute.

This work was supported in part by funding from the National Institutes of Health (AI064811 to W.L. Havran) and the

Skaggs Graduate School of Chemical and Biological Sciences, Scripps Research Institute.

Author contributions: J.M. McGraw, T.S. Young, W.L. Havran, and D.A. Witherden conceived the overall project, designed experiments, and analyzed data. J.M. McGraw, F. Thelen, N.E. Bruno, and D.A. Witherden performed experiments. E.N. Hampton produced functional grade HL4E10 for in vivo studies. J.M. McGraw, T.S. Young, and D.A. Witherden prepared the manuscript.

Disclosures: T.S. Young reported grants from AbbVie during the conduct of the study, and personal fees from AbbVie, Shoreline Bio, and Qihan Bio outside the submitted work. No other disclosures were reported.

Submitted: 11 December 2020
Revised: 28 May 2021
Accepted: 6 August 2021

References

Anders, M., M. Vieth, C. Röcken, M. Ebert, M. Pross, S. Gretschel, P.M. Schlag, B. Wiedenmann, W. Kemmner, and M. Höcker. 2009. Loss of the coxsackie and adenovirus receptor contributes to gastric cancer progression. *Br. J. Cancer*. 100:352–359. https://doi.org/10.1038/sj.bjc.6604876

Badal, B., A. Solovyov, S. Di Cecilia, J.M. Chan, L.-W. Chang, R. Iqbal, I.T. Aydin, G.S. Rajan, C. Chen, F. Abbate, et al. 2017. Transcriptional dissection of melanoma identifies a high-risk subtype underlying TP53 family genes and epigenome deregulation. *JCI Insight*. 2:e92102. https://doi.org/10.1172/jci.insight.92102

Bergelson, J.M., J.A. Cunningham, G. Droguett, E.A. Kurt-Jones, A. Krithivas, J.S. Hong, M.S. Horwitz, R.L. Crowell, and R.W. Finberg. 1997. Isolation of a common receptor for Coxsackie B viruses and adenoviruses 2 and 5. *Science*. 275:1320–1323. https://doi.org/10.1126/science.275.5304.1320

Chen, D.S., and I. Mellman. 2017. Elements of cancer immunity and the cancer-immune set point. *Nature*. 541:321–330. https://doi.org/10.1038/nature21349

Chen, J., S. Li, Q. Yao, N. Du, X. Fu, Y. Lou, M. Wang, F. Mao, D. Mao, P.A. Khadaroo, and Y. Tang. 2020. The efficacy and safety of combined immune checkpoint inhibitors (nivolumab plus ipilimumab): a systematic review and meta-analysis. *World J. Surg. Oncol.* 18:150. https://doi.org/10.1186/s12957-020-01933-5

Clarke, J., B. Panwar, A. Madrigal, D. Singh, R. Gujar, O. Wood, S.J. Chee, S. Eschweiler, E.V. King, A.S. Awad, et al. 2019. Single-cell transcriptomic analysis of tissue-resident memory T cells in human lung cancer. *J. Exp. Med.* 216:2128–2149. https://doi.org/10.1084/jem.20190249

Flesher, J.L., E.K. Paterson-Coleman, P. Vasudeva, R. Ruiz-Vega, M. Marshall, E. Pearlman, G.R. MacGregor, J. Neumann, and A.K. Ganesan. 2020. Delineating the role of MITF isoforms in pigmentation and tissue homeostasis. *Pigment Cell Melanoma Res.* 33:279–292. https://doi.org/10.1111/pcmr.12828

Gao, Y., W. Yang, M. Pan, E. Scully, M. Girardi, L.H. Augenlicht, J. Craft, and Z. Yin. 2003. γ δ T cells provide an early source of interferon γ in tumor immunity. *J. Exp. Med.* 198:433–442. https://doi.org/10.1084/jem.20030584

Garbe, C., T.K. Eigentler, U. Keilholz, A. Hauschild, and J.M. Kirkwood. 2011. Systematic review of medical treatment in melanoma: current status and future prospects. *Oncologist*. 16:5–24. https://doi.org/10.1634/theoncologist.2010-0190

Gentles, A.J., A.M. Newman, C.L. Liu, S.V. Bratman, W. Feng, D. Kim, V.S. Nair, Y. Xu, A. Khuong, C.D. Hoang, et al. 2015. The prognostic landscape of genes and infiltrating immune cells across human cancers. *Nat. Med.* 21:938–945. https://doi.org/10.1038/nm.3909

Girardi, M., D.E. Oppenheim, C.R. Steele, J.M. Lewis, E. Glusac, R. Filler, P. Hobby, B. Sutton, R.E. Tigelaar, and A.C. Hayday. 2001. Regulation of cutaneous malignancy by gammadelta T cells. *Science*. 294:605–609. https://doi.org/10.1126/science.1063916

Guo, Y.L., R. Bai, C.X.J. Chen, D.Q. Liu, Y. Liu, C.Y. Zhang, and K. Zen. 2009. Role of junctional adhesion molecule-like protein in mediating monocyte transendothelial migration. *Arterioscler. Thromb. Vasc. Biol.* 29:75–83. https://doi.org/10.1161/ATVBAHA.108.177717

Hanniford, D., A. Ulloa-Morales, A. Karz, M.G. Berzoti-Coelho, R.S. Moubarak, B. Sánchez-Sendra, A. Kloetgen, V. Davalos, J. Imig, P. Wu, et al. 2020. Epigenetic silencing of CDR1as drives IGF2BP3-mediated melanoma invasion and metastasis. *Cancer Cell*. 37:55–70.e15. https://doi.org/10.1016/j.ccell.2019.12.007

He, W., J. Hao, S. Dong, Y. Gao, J. Tao, H. Chi, R. Flavell, R.L. O'Brien, W.K. Born, J. Craft, et al. 2010. Naturally activated V γ 4 γ δ T cells play a protective role in tumor immunity through expression of eomesodermin. *J. Immunol.* 185:126–133. https://doi.org/10.4049/jimmunol.0903767

Ito, M., M. Kodama, M. Masuko, M. Yamaura, K. Fuse, Y. Uesugi, S. Hirono, Y. Okura, K. Kato, Y. Hotta, et al. 2000. Expression of coxsackievirus and adenovirus receptor in hearts of rats with experimental autoimmune myocarditis. *Circ. Res.* 86:275–280. https://doi.org/10.1161/01.RES.86.3.275

Juneja, V.R., K.A. McGuire, R.T. Manguso, M.W. LaFleur, N. Collins, W.N. Haining, G.J. Freeman, and A.H. Sharpe. 2017. PD-L1 on tumor cells is sufficient for immune evasion in immunogenic tumors and inhibits CD8 T cell cytotoxicity. *J. Exp. Med.* 214:895–904. https://doi.org/10.1084/jem.20160801

Kummer, D., and K. Ebnet. 2018. Junctional adhesion molecules (JAMs): the JAM-integrin connection. *Cells*. 7:25. https://doi.org/10.3390/cells7040025

Lacher, M.D., M.I. Tiirikainen, E.F. Saunier, C. Christian, M. Anders, M. Oft, A. Balmain, R.J. Akhurst, and W.M. Korn. 2006. Transforming growth factor-β receptor inhibition enhances adenoviral infectability of carcinoma cells via up-regulation of Coxsackie and Adenovirus Receptor in conjunction with reversal of epithelial-mesenchymal transition. *Cancer Res.* 66:1648–1657. https://doi.org/10.1158/0008-5472.CAN-05-2328

Larkin, J., V. Chiarion-Sileni, R. Gonzalez, J.J. Grob, C.L. Cowey, C.D. Lao, D. Schadendorf, R. Dummer, M. Smylie, P. Rutkowski, et al. 2015. Combined nivolumab and ipilimumab or monotherapy in untreated melanoma. *N. Engl. J. Med.* 373:23–34. https://doi.org/10.1056/NEJMoa1504030

Larkin, J., V. Chiarion-Sileni, R. Gonzalez, J.J. Grob, P. Rutkowski, C.D. Lao, C.L. Cowey, D. Schadendorf, J. Wagstaff, R. Dummer, et al. 2019. Five-year survival with combined nivolumab and ipilimumab in advanced melanoma. *N. Engl. J. Med.* 381:1535–1546. https://doi.org/10.1056/NEJMoa1910836

Lauko, A., Z. Mu, D.H. Gutmann, U.P. Naik, and J.D. Lathia. 2020. Junctional adhesion molecules in cancer: a paradigm for the diverse functions of cell-cell interactions in tumor progression. *Cancer Res.* 80:4878–4885. https://doi.org/10.1158/0008-5472.CAN-20-1829

Lee, P.-H., T.N. Yamamoto, D. Gurusamy, M. Sukumar, Z. Yu, J. Hu-Li, T. Kawabe, A. Gangaplara, R.J. Kishton, A.N. Henning, et al. 2019. Host conditioning with IL-1β improves the antitumor function of adoptively transferred T cells. *J. Exp. Med.* 216:2619–2634. https://doi.org/10.1084/jem.20181218

Li, D., L. Duan, P. Freimuth, and B.W. O'Malley Jr. 1999a. Variability of adenovirus receptor density influences gene transfer efficiency and therapeutic response in head and neck cancer. *Clin. Cancer Res.* 5:4175–4181.

Li, Y., R.C. Pong, J.M. Bergelson, M.C. Hall, A.I. Sagalowsky, C.P. Tseng, Z. Wang, and J.T. Hsieh. 1999b. Loss of adenoviral receptor expression in human bladder cancer cells: a potential impact on the efficacy of gene therapy. *Cancer Res.* 59:325–330.

Li, B., E. Severson, J.C. Pignon, H. Zhao, T. Li, J. Novak, P. Jiang, H. Shen, J.C. Aster, S. Rodig, et al. 2016. Comprehensive analyses of tumor immunity: implications for cancer immunotherapy. *Genome Biol.* 17:174. https://doi.org/10.1186/s13059-016-1028-7

Li, J., Y. He, J. Hao, L. Ni, and C. Dong. 2018. High levels of Eomes promote exhaustion of anti-tumor CD8$^+$ T cells. *Front. Immunol.* 9:2981. https://doi.org/10.3389/fimmu.2018.02981

Liu, D., B. Schilling, D. Liu, A. Sucker, E. Livingstone, L. Jerby-Arnon, L. Zimmer, R. Gutzmer, I. Satzger, C. Loquai, et al. 2019. Integrative molecular and clinical modeling of clinical outcomes to PD1 blockade in patients with metastatic melanoma. *Nat. Med.* 25:1916–1927. https://doi.org/10.1038/s41591-019-0654-5

Luissint, A.C., P.G. Lutz, D.A. Calderwood, P.O. Couraud, and S. Bourdoulous. 2008. JAM-L-mediated leukocyte adhesion to endothelial cells is regulated in cis by $\alpha_4\beta_1$ integrin activation. *J. Cell Biol.* 183:1159–1173. https://doi.org/10.1083/jcb.200805061

Mackay, L.K., A. Rahimpour, J.Z. Ma, N. Collins, A.T. Stock, M.L. Hafon, J. Vega-Ramos, P. Lauzurica, S.N. Mueller, T. Stefanovic, et al. 2013. The

developmental pathway for CD103(+)CD8+ tissue-resident memory T cells of skin. *Nat. Immunol.* 14:1294–1301. https://doi.org/10.1038/ni.2744

Matsumoto, K., S.F. Shariat, G.E. Ayala, K.A. Rauen, and S.P. Lerner. 2005. Loss of coxsackie and adenovirus receptor expression is associated with features of aggressive bladder cancer. *Urology.* 66:441–446. https://doi.org/10.1016/j.urology.2005.02.033

Mayes, P.A., K.W. Hance, and A. Hoos. 2018. The promise and challenges of immune agonist antibody development in cancer. *Nat. Rev. Drug Discov.* 17:509–527. https://doi.org/10.1038/nrd.2018.75

Moog-Lutz, C., F. Cavé-Riant, F.C. Guibal, M.A. Breau, Y. Di Gioia, P.O. Couraud, Y.E. Cayre, S. Bourdoulous, and P.G. Lutz. 2003. JAML, a novel protein with characteristics of a junctional adhesion molecule, is induced during differentiation of myeloid leukemia cells. *Blood.* 102: 3371–3378. https://doi.org/10.1182/blood-2002-11-3462

Nielsen, M.M., D.A. Witherden, and W.L. Havran. 2017. γδ T cells in homeostasis and host defence of epithelial barrier tissues. *Nat. Rev. Immunol.* 17:733–745. https://doi.org/10.1038/nri.2017.101

Nilchian, A., J. Johansson, A. Ghalali, S.T. Asanin, A. Santiago, O. Rosencrantz, K. Sollerbrant, C.T. Vincent, M. Sund, U. Stenius, and J. Fuxe. 2019. CXADR-mediated formation of an AKT inhibitory signalosome at tight junctions controls epithelial-mesenchymal plasticity in breast cancer. *Cancer Res.* 79:47–60. https://doi.org/10.1158/0008-5472.CAN-18-1742

Ortiz-Zapater, E., G. Santis, and M. Parsons. 2017. CAR: A key regulator of adhesion and inflammation. *Int. J. Biochem. Cell Biol.* 89:1–5. https://doi.org/10.1016/j.biocel.2017.05.025

Paley, M.A., D.C. Kroy, P.M. Odorizzi, J.B. Johnnidis, D.V. Dolfi, B.E. Barnett, E.K. Bikoff, E.J. Robertson, G.M. Lauer, S.L. Reiner, and E.J. Wherry. 2012. Progenitor and terminal subsets of CD8+ T cells cooperate to contain chronic viral infection. *Science.* 338:1220–1225. https://doi.org/10.1126/science.1229620

Postow, M.A., J. Chesney, A.C. Pavlick, C. Robert, K. Grossmann, D. McDermott, G.P. Linette, N. Meyer, J.K. Giguere, S.S. Agarwala, et al. 2015. Nivolumab and ipilimumab versus ipilimumab in untreated melanoma. *N. Engl. J. Med.* 372:2006–2017. https://doi.org/10.1056/NEJMoa1414428

Rashidian, M., M.W. LaFleur, V.L. Verschoor, A. Dongre, Y. Zhang, T.H. Nguyen, S. Kolifrath, A.R. Aref, C.J. Lau, C.P. Paweletz, et al. 2019. Immuno-PET identifies the myeloid compartment as a key contributor to the outcome of the antitumor response under PD-1 blockade. *Proc. Natl. Acad. Sci. USA.* 116:16971–16980. https://doi.org/10.1073/pnas.1905005116

Reeh, M., M. Bockhorn, D. Görgens, M. Vieth, T. Hoffmann, R. Simon, J.R. Izbicki, G. Sauter, U. Schumacher, and M. Anders. 2013. Presence of the coxsackievirus and adenovirus receptor (CAR) in human neoplasms: a multitumour array analysis. *Br. J. Cancer.* 109:1848–1858. https://doi.org/10.1038/bjc.2013.509

Ribot, J.C., A. Debarros, L. Mancio-Silva, A. Pamplona, and B. Silva-Santos. 2012. B7-CD28 costimulatory signals control the survival and proliferation of murine and human γδ T cells via IL-2 production. *J. Immunol.* 189: 1202–1208. https://doi.org/10.4049/jimmunol.1200268

Schultz, L., and C. Mackall. 2019. Driving CAR T cell translation forward. *Sci. Transl. Med.* 11:eaaw2127. https://doi.org/10.1126/scitranslmed.aaw2127

Silva-Santos, B., S. Mensurado, and S.B. Coffelt. 2019. γδ T cells: pleiotropic immune effectors with therapeutic potential in cancer. *Nat. Rev. Cancer.* 19:392–404. https://doi.org/10.1038/s41568-019-0153-5

Talantov, D., A. Mazumder, J.X. Yu, T. Briggs, Y. Jiang, J. Backus, D. Atkins, and Y. Wang. 2005. Novel genes associated with malignant melanoma but not benign melanocytic lesions. *Clin. Cancer Res.* 11:7234–7242. https://doi.org/10.1158/1078-0432.CCR-05-0683

Thommen, D.S., and T.N. Schumacher. 2018. T cell dysfunction in cancer. *Cancer Cell.* 33:547–562. https://doi.org/10.1016/j.ccell.2018.03.012

Verdino, P., D.A. Witherden, W.L. Havran, and I.A. Wilson. 2010. The molecular interaction of CAR and JAML recruits the central cell signal transducer PI3K. *Science.* 329:1210–1214. https://doi.org/10.1126/science.1187996

Verdino, P., D.A. Witherden, K. Podshivalova, S.E. Rieder, W.L. Havran, and I.A. Wilson. 2011. cDNA sequence and Fab crystal structure of HL4E10, a hamster IgG lambda light chain antibody stimulatory for γδ T cells. *PLoS One.* 6:e19828. https://doi.org/10.1371/journal.pone.0019828

Vincent, T., R.F. Pettersson, R.G. Crystal, and P.L. Leopold. 2004. Cytokine-mediated downregulation of coxsackievirus-adenovirus receptor in endothelial cells. *J. Virol.* 78:8047–8058. https://doi.org/10.1128/JVI.78.15.8047-8058.2004

Witherden, D.A., P. Verdino, S.E. Rieder, O. Garijo, R.E. Mills, L. Teyton, W.H. Fischer, I.A. Wilson, and W.L. Havran. 2010. The junctional adhesion molecule JAML is a costimulatory receptor for epithelial gammadelta T cell activation. *Science.* 329:1205–1210. https://doi.org/10.1126/science.1192698

Yamashita, M., A. Ino, K. Kawabata, F. Sakurai, and H. Mizuguchi. 2007. Expression of coxsackie and adenovirus receptor reduces the lung metastatic potential of murine tumor cells. *Int. J. Cancer.* 121:1690–1696. https://doi.org/10.1002/ijc.22852

Yost, K.E., A.T. Satpathy, D.K. Wells, Y. Qi, C. Wang, R. Kageyama, K.L. McNamara, J.M. Granja, K.Y. Sarin, R.A. Brown, et al. 2019. Clonal replacement of tumor-specific T cells following PD-1 blockade. *Nat. Med.* 25:1251–1259. https://doi.org/10.1038/s41591-019-0522-3

Zen, K., Y. Liu, I.C. McCall, T. Wu, W. Lee, B.A. Babbin, A. Nusrat, and C.A. Parkos. 2005. Neutrophil migration across tight junctions is mediated by adhesive interactions between epithelial coxsackie and adenovirus receptor and a junctional adhesion molecule-like protein on neutrophils. *Mol. Biol. Cell.* 16:2694–2703. https://doi.org/10.1091/mbc.e05-01-0036

Zussy, C., F. Loustalot, F. Junyent, F. Gardoni, C. Bories, J. Valero, M.G. Desarménien, F. Bernex, D. Henaff, N. Bayo-Puxan, et al. 2016. Coxsackievirus adenovirus receptor loss impairs adult neurogenesis, synapse content, and hippocampus plasticity. *J. Neurosci.* 36:9558–9571. https://doi.org/10.1523/JNEUROSCI.0132-16.2016

Supplemental material

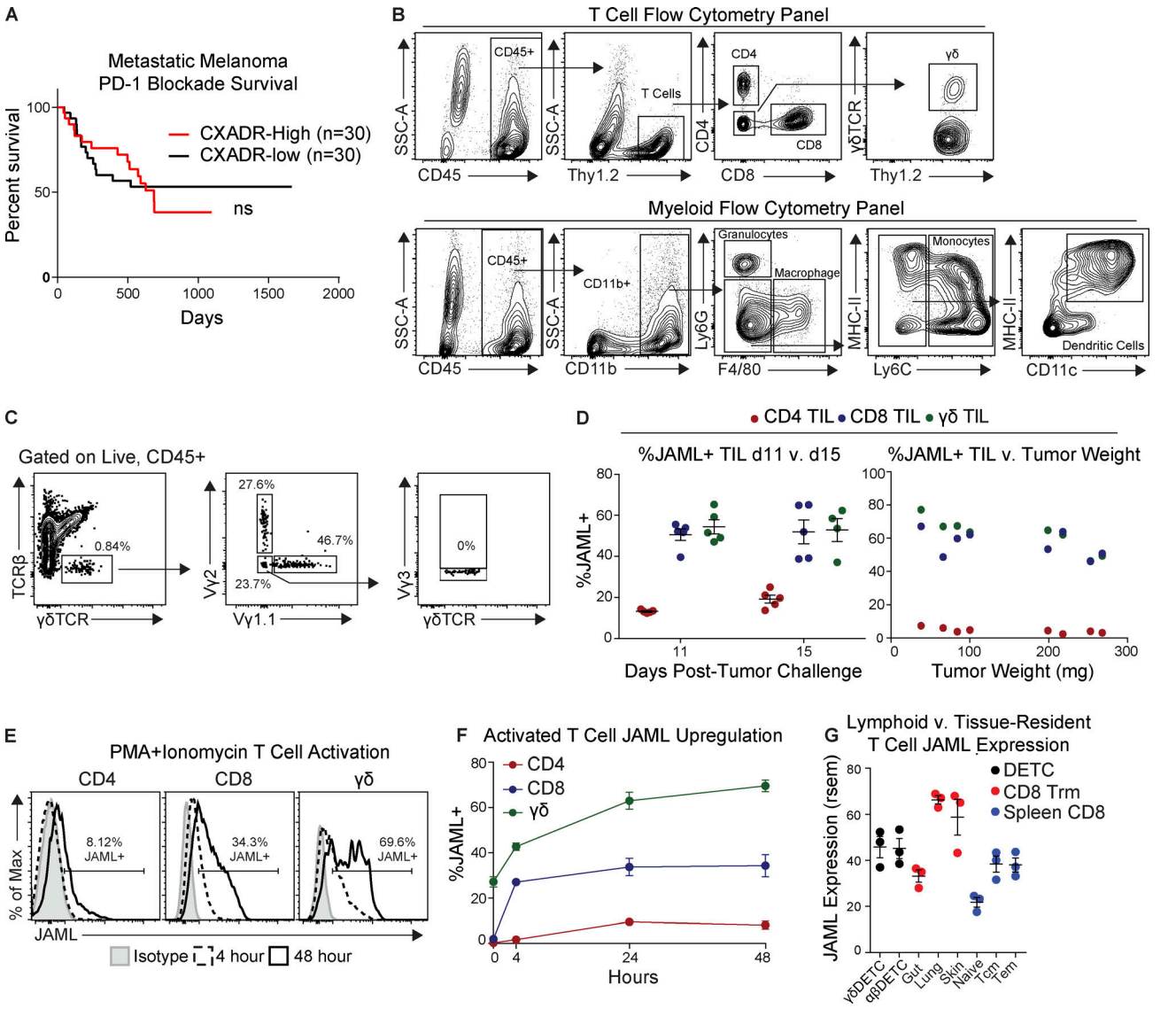

Figure S1. **Association of CXADR expression with response to PD-1 blockade and additional characterization of mouse CD8 and γδ T cell JAML expression. (A)** The association between CXADR expression in metastatic melanoma lesions before anti–PD-1 therapy and clinical outcomes was analyzed in a previously published dataset (Liu et al., 2019). Kaplan-Meier plot of metastatic melanoma patients within the top and bottom quartiles of *CXADR* expression. **(B–D)** B16F10 tumor tissue was isolated from WT mice on either day 11 or 15 after tumor challenge and analyzed by flow cytometry. **(B)** Representative flow cytometry gating of T cell and myeloid cell subsets on day 15 after tumor challenge. SSC-A, side scatter area. **(C)** Representative flow cytometry gating of γδ TIL subsets on day 15 after tumor challenge. **(D)** Frequency of JAML$^+$ CD4, CD8, and γδ TILs on day 11 and day 15 after tumor challenge (n = 4–5/time point) and in relation to tumor weight (n = 7–8). **(E and F)** Splenocytes were isolated from naive WT mice; stimulated ex vivo with PMA and ionomycin for 4, 24, or 48 h; and then analyzed by flow cytometry. (E) Representative histograms and (F) frequency of JAML expression by CD4, CD8, and γδ T cells (n = 4/time point). **(G)** Gene expression by lymphoid and tissue-resident T cell subsets was analyzed in the GEO accession no. GSE47045 dataset. *Jaml* mRNA expression by DETCs, CD8 tissue-resident memory (Trm), and lymphoid CD8 T cell subsets (n = 3/group). Data in B–F are representative of at least three independent experiments. Data in D, F, and G are expressed as mean ± SEM. Tcm, central memory T cell; Tem, effector memory T cell.

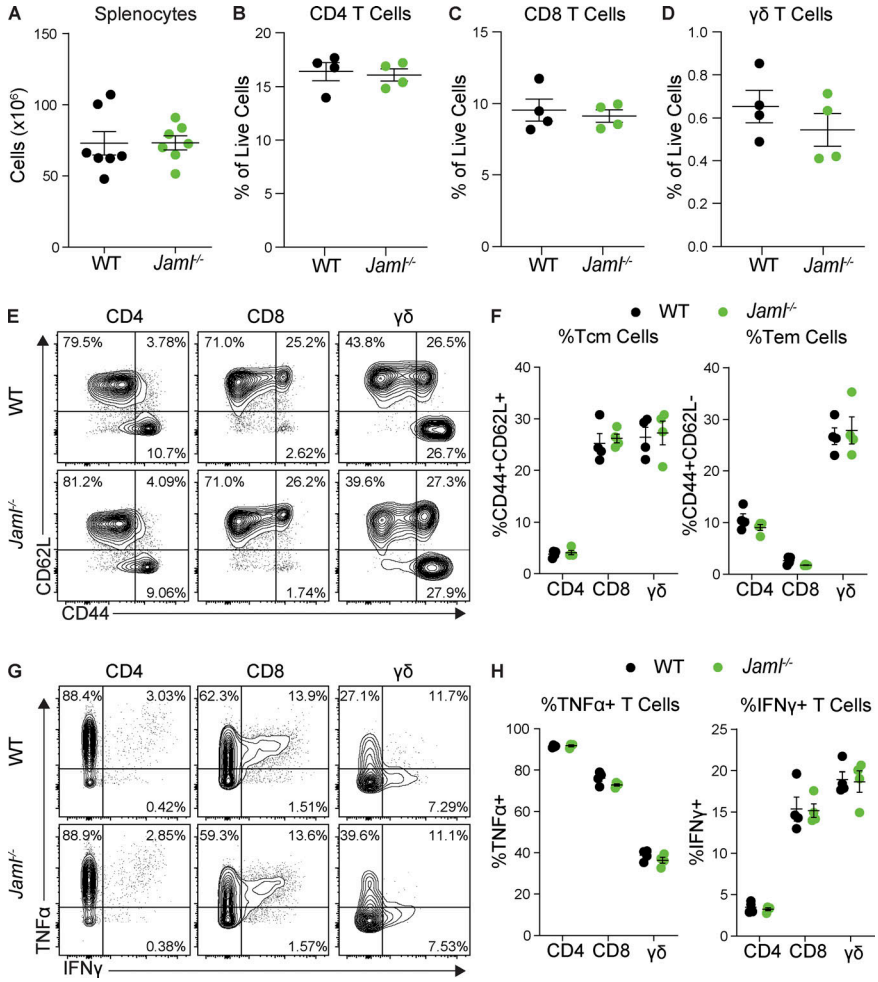

Figure S2. **Analysis of T cell splenocytes in naive WT versus *Jaml*$^{-/-}$ mice. (A–H)** Splenocytes were isolated from naive 8-wk-old WT and *Jaml*$^{-/-}$ mice and analyzed by flow cytometry. **(A)** Total splenocyte numbers (n = 7/group). **(B–D)** Frequency of (B) CD4, (C) CD8, and (D) γδ T cells (n = 4/group). **(E and F)** (E) Representative flow cytometry plots of CD44 versus CD62L expression and (F) frequency of central memory (Tcm) and effector memory (Tem) T cell subsets (n = 4/group). **(G and H)** (G) Representative flow cytometry plots and (H) frequency of TNFα and IFNγ production by splenic T cells following ex vivo stimulation with PMA and ionomycin (n = 4/group). Data are expressed as mean ± SEM and are representative of two independent experiments.

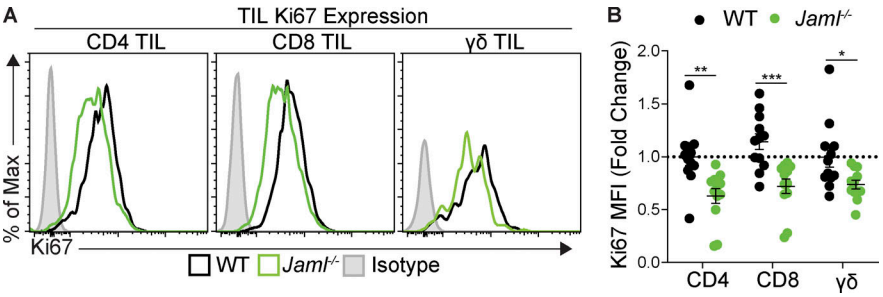

Figure S3. **Characterization of Ki67 expression by TILs in WT versus *Jaml*$^{-/-}$ mice on day 15 after B16F10 tumor challenge. (A and B)** Tumor tissue was isolated from WT and *Jaml*$^{-/-}$ mice on day 15 after B16F10 tumor challenge and analyzed by flow cytometry. (A) Representative histograms and (B) quantification of Ki67 MFI by CD4, CD8, and γδ TILs (fold change compared with WT CD4 TIL mean; n = 12/group). Data are expressed as mean ± SEM and represent combined data from three experiments. *, P < 0.05; **, P < 0.01; ***, P < 0.001; Student's t test.

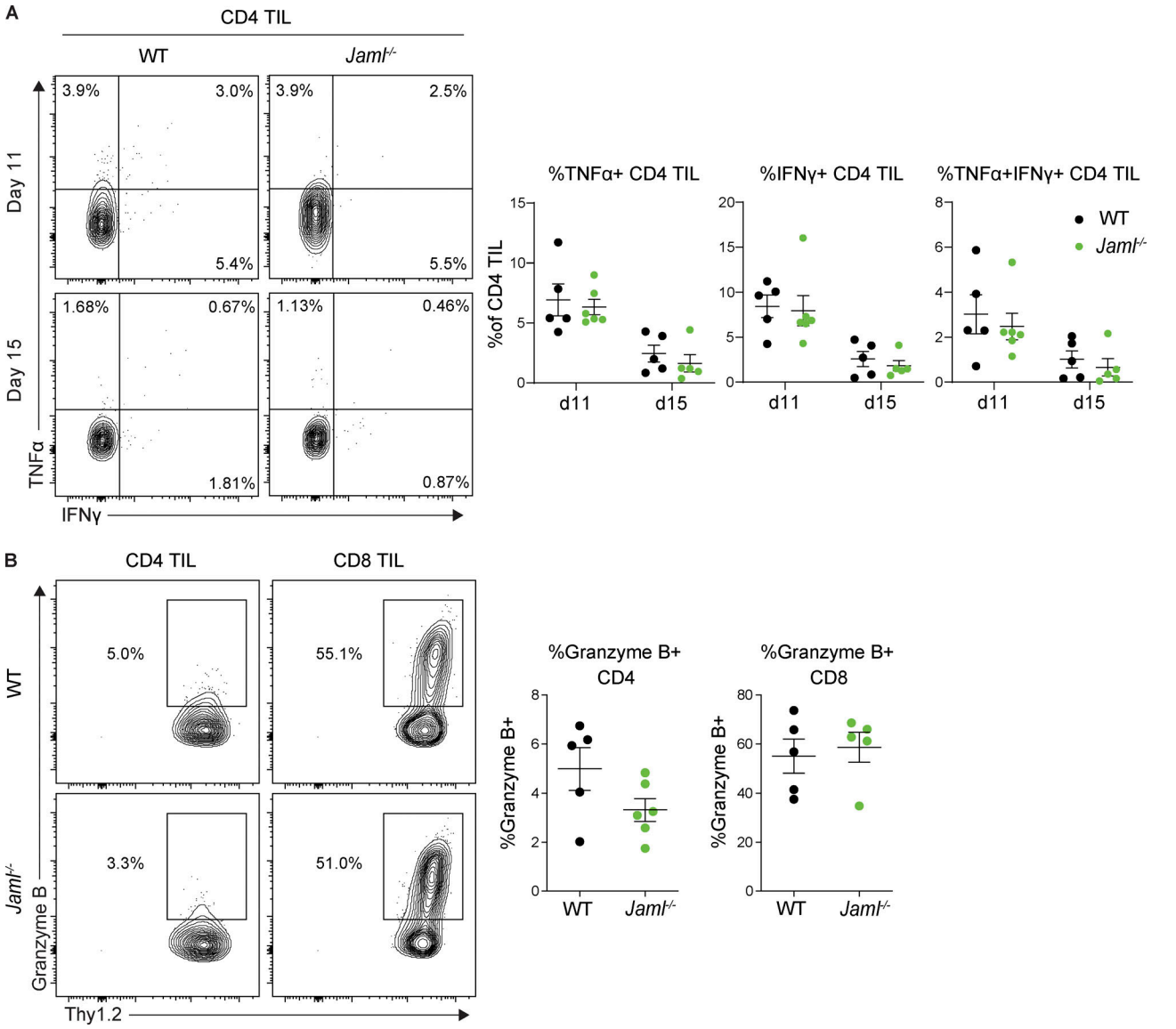

Figure S4. **Ex vivo cytokine production by CD4 and CD8 TILs in WT versus *Jaml*$^{-/-}$ mice. (A and B)** Tumor tissue was isolated from WT and *Jaml*$^{-/-}$ mice on day 11 or 15 after B16F10 tumor challenge and analyzed by flow cytometry following ex vivo stimulation (WT, $n = 5$; *Jaml*$^{-/-}$, $n = 5–6$). **(A)** Representative flow cytometry plots and frequency of TNFα and IFNγ production by CD4 TILs on days 11 and 15 after tumor challenge. **(B)** Representative flow cytometry plots and frequency of granzyme B production by CD4 and CD8 TILs on day 11 after tumor challenge. Data are expressed as mean ± SEM and are representative of at least three independent experiments.

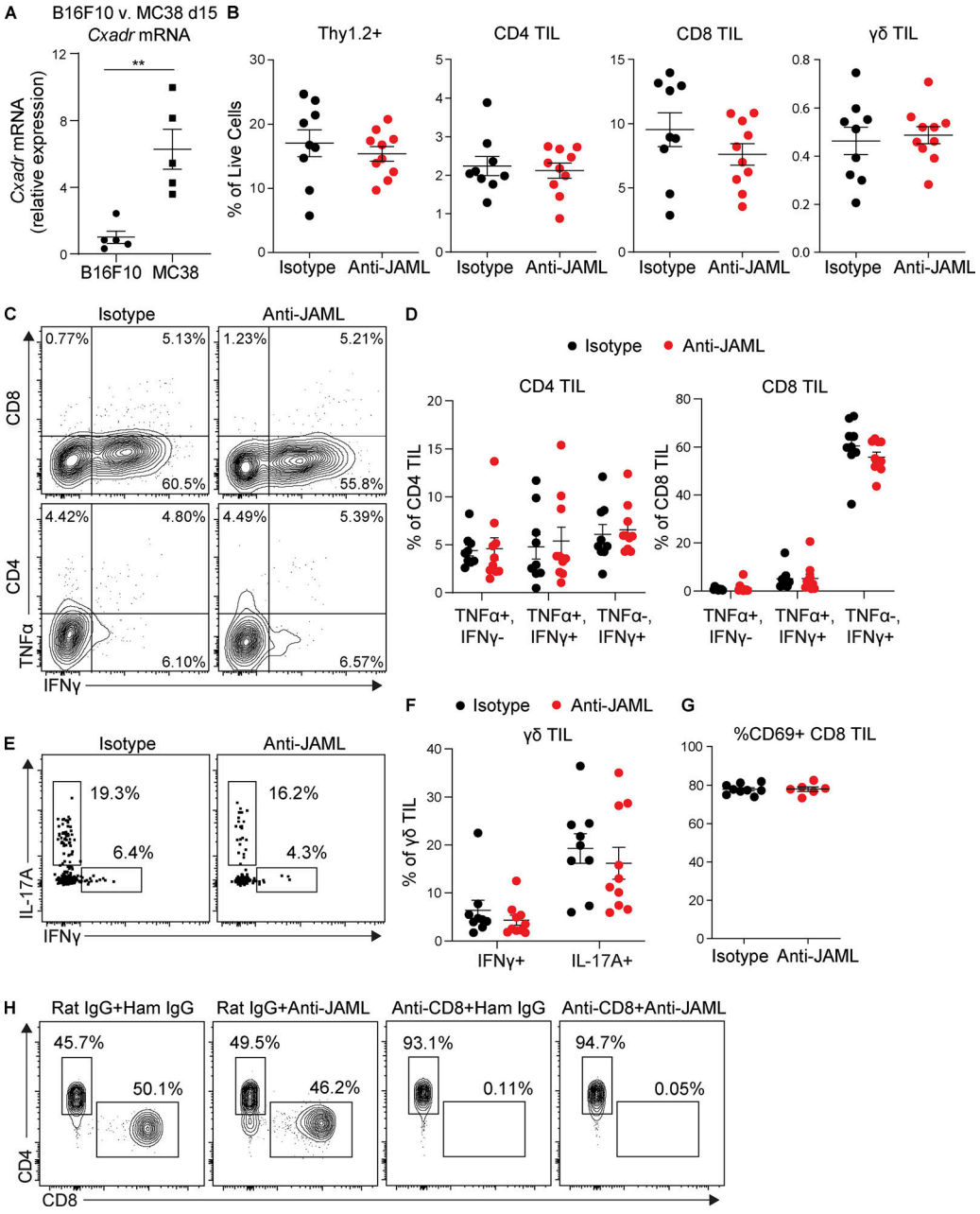

Figure S5. **B16F10 versus MC38 tumor *Cxadr* mRNA expression and B16F10 TIL numbers and cytokine production following anti-JAML treatment.** **(A)** B16F10 and MC38 tumor tissue was isolated from WT mice on day 15 after tumor challenge. Bulk tumor mRNA was isolated and analyzed by quantitative PCR. *Cxadr* mRNA expression in B16F10 versus MC38 tumor tissue (n = 5/group). **(B–G)** WT mice were challenged with B16F10 melanoma and treated with isotype IgG or anti-JAML antibodies on day 7 after tumor challenge. Tumor tissue was isolated on day 12 after tumor challenge and analyzed by flow cytometry. **(B)** Frequency of Thy1.2$^+$, CD4$^+$, CD8$^+$, and γδTCR$^+$ TILs. **(C and D)** (C) Representative flow cytometry plots and (D) frequency of TNFα and IFNγ production by CD4 and CD8 TILs following ex vivo stimulation. **(E and F)** (E) Representative flow cytometry plots and (F) frequency of IFNγ and IL-17A by γδ TILs following ex vivo stimulation. **(G)** Frequency of CD69 expression by CD8 TILs (isotype IgG, n = 9; anti-JAML, n = 6). **(H)** WT mice were challenged with B16F10 melanoma and treated with isotype IgG or anti-JAML antibodies and isotype IgG or anti-CD8 depleting antibodies on days 7 and 10 after tumor challenge. Peripheral blood was collected on day 11 after tumor challenge and analyzed by flow cytometry. Representative flow cytometry plots of CD4 and CD8 T cells. Ham, hamster. Data in A–H are representative of two independent experiments. Data in A, B, D, F, and G are expressed as mean ± SEM (B, D, and F; n = 9 isotype; n = 10 anti-JAML). **(A)** **, $P < 0.01$; Student's t test.